Mice lacking *ARV1* have reduced signs of metabolic syndrome and non-alcoholic fatty liver disease

Received for publication, November 4, 2017, and in revised form, February 27, 2018 Published, Papers in Press, February 28, 2018, DOI 10.1074/jbc.RA117.000800

Christina Gallo-Ebert[‡], Jamie Francisco[‡], Hsing-Yin Liu[‡], Riley Draper[§], Kinnari Modi[‡], Michael D. Hayward[¶], Beverly K. Jones[¶], Olesia Buiakova[¶], Virginia McDonough[§], and Joseph T. Nickels, Jr.[‡‖1]

From the [‡]Institute of Metabolic Disorders, Genesis Biotechnology Group, Hamilton, New Jersey 08691, [§]Hope College, Holland, Michigan 49423, [¶]Invivotek, Genesis Biotechnology Group, Hamilton, New Jersey 08691, and the [‖]Rutgers Center for Lipid Research, New Jersey Institute for Food, Nutrition, and Health, Rutgers University, New Brunswick, New Jersey 08901

Edited by Jeffrey E. Pessin

Metabolic syndrome (MetS) is a term used to characterize individuals having at least three of the following diseases: obesity, dyslipidemia, hyperglycemia, insulin resistance, hypertension, and nonalcoholic fatty liver disease (NAFLD). It is widespread, and the number of individuals with MetS is increasing. However, the events leading to the manifestation of MetS are not well-understood. Here, we show that loss of murine *ARV1* (*mARV1*) results in resistance to acquiring diseases associated with MetS. *Arv1*$^{-/-}$ animals fed a high-fat diet were resistant to diet-induced obesity, had lower blood cholesterol and triglyceride levels, and retained glucose tolerance and insulin sensitivity. Livers showed no gross morphological changes, contained lower levels of cholesterol, triglycerides, and fatty acids, and showed fewer signs of NAFLD. Knockout animals had elevated levels of liver farnesol X receptor (FXR) protein and its target, small heterodimer protein (SHP). They also had decreased levels of CYP7α1, CYP8β1, and mature SREBP1 protein, evidence suggesting that liver FXR signaling was activated. Strengthening this hypothesis was the fact that peroxisome proliferator-activating receptor α (PPARα) protein was elevated, along with its target, fibroblast growth factor 21 (FGF21). *Arv1*$^{-/-}$ animals excreted more fecal cholesterol, free fatty acids, and bile acids. Their small intestines had 1) changes in bile acid composition, 2) an increase in the level of the intestinal FXR antagonist, tauromuricholic acid, and 3) showed signs of attenuated FXR signaling. Overall, we believe that ARV1 function is deleterious when consuming a high-fat diet. We further hypothesize that ARV1 is critical for initiating events required for the progression of diseases associated with MetS and NAFLD.

Approximately 20–30% of the world's population has pathologies that are associated with MetS.[2] MetS is a term used for a set of diseases that includes obesity, type 2 diabetes (T2D), hyperlipidemia, hypertension, insulin resistance, and NAFLD (1). Health consequences include premature death due to T2D-related cardiovascular disease and stroke and obesity-related increases in the levels of lipids associated with atherosclerosis and certain cancers (2, 3). It is estimated that by the year 2030, 60% of individuals will be characterized as having MetS (4).

Obesity is thought to be the main driver for progressing the severity of MetS (5). However, about one-third of obese individuals are metabolically healthy, so the etiology is not completely clear-cut and suggests a genetic predisposition to the disease (6). There is a debate whether NAFLD precedes the onset of MetS or requires the presence of one or more of its diseases to progress (7, 8). NAFLD is prevalent among the world's population at least in part due to the emergence of a Western diet that is high in saturated fats and refined sugars (9). It can progress to nonalcoholic steatohepatitis → fibrosis → cirrhosis → hepatic cancer (10). NAFLD is thought to be due to the deposition of fatty acids from adipose to the liver and subsequent accumulation of triglycerides (11). There are data that suggest insulin resistance precedes NAFLD and is required for the manifestation of the disease (10), as it causes a dysregulation of lipogenic and lipolytic activities in the liver and adipose tissue, respectively (12). Thus, whereas the diseases associated with MetS are known, their relationships to the onset and progression of NALD are not well-understood.

ARV1 (ARE1 ARE2 required for viability 1) was first identified in *S. cerevisiae* using a screen searching for genes required for viability in the absence of sterol esterification (13). *S. cerevisiae* cells lacking *ARV1* have defects in phospholipid, sphingolipid, glycosylphosphatidylinositol, and sterol syntheses, and lack the ability to localize sterol and mobilize phosphatidylinositol 4,5-bisphosphate (13–16). *arv1*-deficient cells are hypersensitive to the phosphatidylserine-binding agent, papu-

This work was supported by the Genesis Biotechnology Group. The authors declare that they have no conflicts of interest with the contents of this article.

This article contains Figs. S1–S6.

[1] To whom correspondence should be addressed: Institute of Metabolic Disorders, Genesis Biotechnology Group, 1000 Waterview Dr., Hamilton, NJ 08691. Tel.: 609-786-2870; Fax: 609-587-1827; E-mail: jnickels@venenumbiodesign.com.

[2] The abbreviations used are: MetS, metabolic syndrome; T2D, type II diabetes; ASO, antisense oligonucleotide; Chol, cholesterol; DGAT, diacylglycerol acyltransferase; DEXA, dual-energy X-ray absorptiometry; DIO, diet-induced obesity; FGF21, fibroblastic growth factor 21; FFA, free fatty acid; FXR, farnesol X receptor; HFD, high-fat diet; ICR, Institute of Cancer Research; KO, knockout; MGAT, monoacylglycerol acyltransferase; NAFLD, non-alcoholic fatty liver disease; NC, normal chow; NKO, *nestin-Cre ARV1* neuronal knockout; OGTT, oral glucose tolerance test; PPARα, peroxisome proliferator-activated receptor α; SI, small intestine; SREBP, sterol response element–binding protein; TAG, triglyceride; TC, taurocholic acid; TDC, taurodeoxycholic acid; TMC, tauromuricholic acid; TUDC, tauroursodeoxycholic acid; VLDL, very low-density lipoprotein cholesterol; H&E, hematoxylin and eosin; hetero, heterozygous; LDL, low-density lipoprotein; HDL, high-density lipoprotein; SCD1, stearoyl-CoA desaturase 1; SHP, small heterodimer protein; ANOVA, analysis of variance.

amide-B, suggesting a mislocalization of phosphatidylserine to the plasma membrane (17). They contain fragmented vacuoles and a disrupted organelle phenotype (17), which most likely activates the unfolded protein response (18). Null cells are hypersensitive to fatty acid supplementation (19), suggesting that Arv1 also regulates fatty acid metabolism. Thus, yeast Arv1 has a major role in regulating lipid synthesis, metabolism, and homeostasis and is needed to rescue cells when these processes become perturbed.

There is evidence that ARV1 regulates lipid distribution and metabolism in mammals. Knockdown of *Arv1* in HepG2 cells results in the accumulation of cholesterol in the endoplasmic reticulum and a reduction in the plasma membrane, suggesting defective sterol transport in the liver (20). Mice treated with antisense oligonucleotides (ASOs) to *Arv1* have increases in plasma and liver bile acid levels that contain hydrophilic bile acid salts (20). The same authors observed that early loss of *Arv1* caused increases in plasma PL, cholesterol, and low-density apolipoprotein–cholesterol levels and a decrease in high-density apolipoprotein–cholesterol levels (20). Interestingly, human ARV1 possesses *in vitro* lipid binding activity, as it binds sterol intermediates (21), several fatty acid species (22), and specific phospholipids and cholesterol.[3]

Recent mouse model studies have presented data exploring the neurological and metabolic phenotypes of neuronal knockout (NKO) and whole-body $Arv1^{-/-}$ animals (23, 24). Palmer *et al.* (24) found that NKO $Arv1^{-/-}$ animals suffered from seizures and epileptic encephalopathy. Lagor *et al.* (23) discovered that $Arv1^{-/-}$ animals displayed multiple beneficial metabolic changes, including lack of weight gain, improved glucose tolerance, elevated adiponectin secretion, increased energy expenditure, and a decrease in white adipose tissue. These studies strongly suggest that Arv1 plays a critical role in maintaining brain function and metabolic homeostasis. Here, we asked how $Arv1^{-/-}$ animals responded to a high-fat diet. Our results indicate that ARV1 function is needed for progressing diseases associated with MetS.

Results

Arv1$^{-/-}$ *mice lack any detectable ARV1 protein*

C57BL/6J-derived ES cells were used to generate $Arv1^{-/-}$ animals. They were maintained on the identical C57BL/6J background, making backcrossing unnecessary. To generate knockout animals, we excised exon 5 from the *Arv1* gene locus (Fig. 1*A*). To test for proper deletion, *Arv1* mRNA transcripts were quantified by quantitative real-time PCR, and ARV1 protein levels were determined by Western blot analysis. Tissues analyzed were liver, brain, small intestine (SI), lung, kidney, and adipose.

The *Arv1* gene encodes an mRNA containing six exons (271 amino acids; 31 kDa) (Fig. 1, *B* and *C*), which expresses a protein that in our hands migrates at 31 kDa by Western blot analysis (Fig. 2). To determine whether $Arv1^{-/-}$ animals expressed any mRNA transcripts, we designed primers able to quantify the

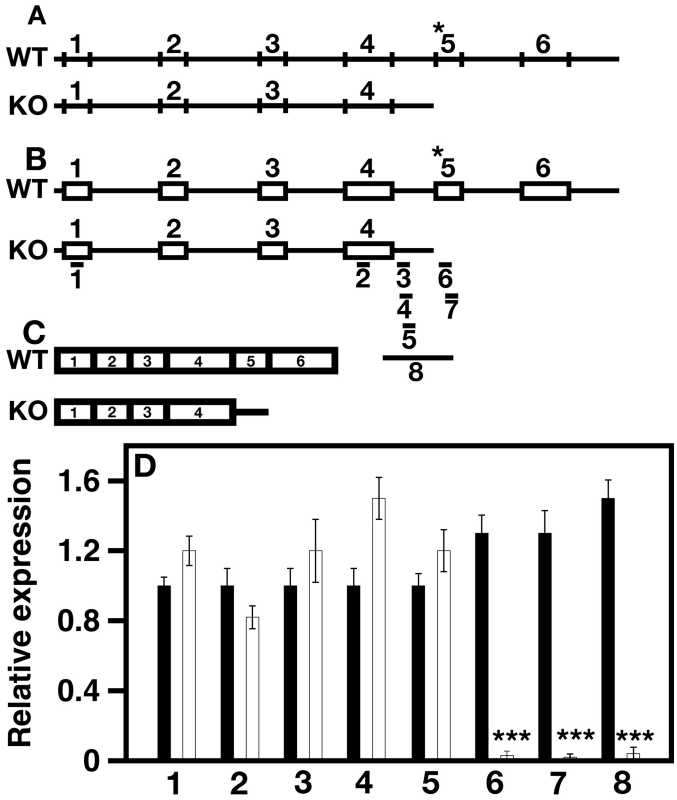

Figure 1. ***Arv1***$^{-/-}$ **animals lack expression of a full-length mRNA containing exon 5.** *A*, arrangement of the *Arv1* gene locus. *Numbers*, *exons*; *lines*, introns. *B*, arrangement of the *Arv1* hnRNA. *Boxes*, exons; *lines*, introns. *C*, organization of the full-length *Arv1* mRNA. *Numbers*, exons. *D*, *ARV1* mRNA expression levels in the liver. *ARV1* mRNA expression was determined using quantitative real-time PCR. *Numbers* in *D* indicate what primers were used, as indicated in *B*. *Black bars*, WT; *white bars*, $Arv1^{-/-}$; ***, $p < 0001$; $n = 8$. *Error bars*, S.E.

levels of exon 1, exon 4, intragenic regions between exons 4 and 5, exon 5, and the contiguous junction between exons 4 and 5 (Fig. 1*B*). We found that $Arv1^{-/-}$ animals expressed a mRNA in liver that contained exons 1–4, along with a portion of downstream intragenic sequences between exons 4 and 5 (Fig. 1*D*, *1–5*). However, we did not detect an mRNA expressing exon 5 (Fig. 1*D*, *6* and *7*) or sequences coding for the contiguous junction between exons 4 and 5 (Fig. 1*D*, *8*). On the other hand, WT animals expressed an mRNA containing exons 1–5 (Fig. 1*B*). Presumably, this WT mRNA is a full-length transcript that contains exon 6 and downstream sequences containing the 3′-UTR and poly(A) tail. These sequences would be absent in the truncated *Arv1* transcript detected in $Arv1^{-/-}$ animals. All other tissues analyzed gave identical results (data not shown).

Based on the quantitative real-time PCR data, $Arv1^{-/-}$ animals could be expressing a truncated form of the ARV1 protein (Fig. 1*C*). We addressed this question by determining the levels of ARV1 protein in several tissues using Western blot analysis. $Arv1^{-/-}$ mice did not express either a full-length or truncated form of ARV1 in any tissue tested, with the exception of one animal, which expressed a low level of full-length ARV1 in the SI (Fig. 2 and Fig. S1). Western blot analysis using SIs from all other knockout animals used in our studies did not show any full-length or truncated ARV1 protein expression (*not shown*). WT animals expressed ARV1 protein in the liver and SI, but we

[3] H.-Y. Liu, C. Gallo-Ebert, K. Modi, J. L. Cunningham, and J. T. Nickels, manuscript in preparation.

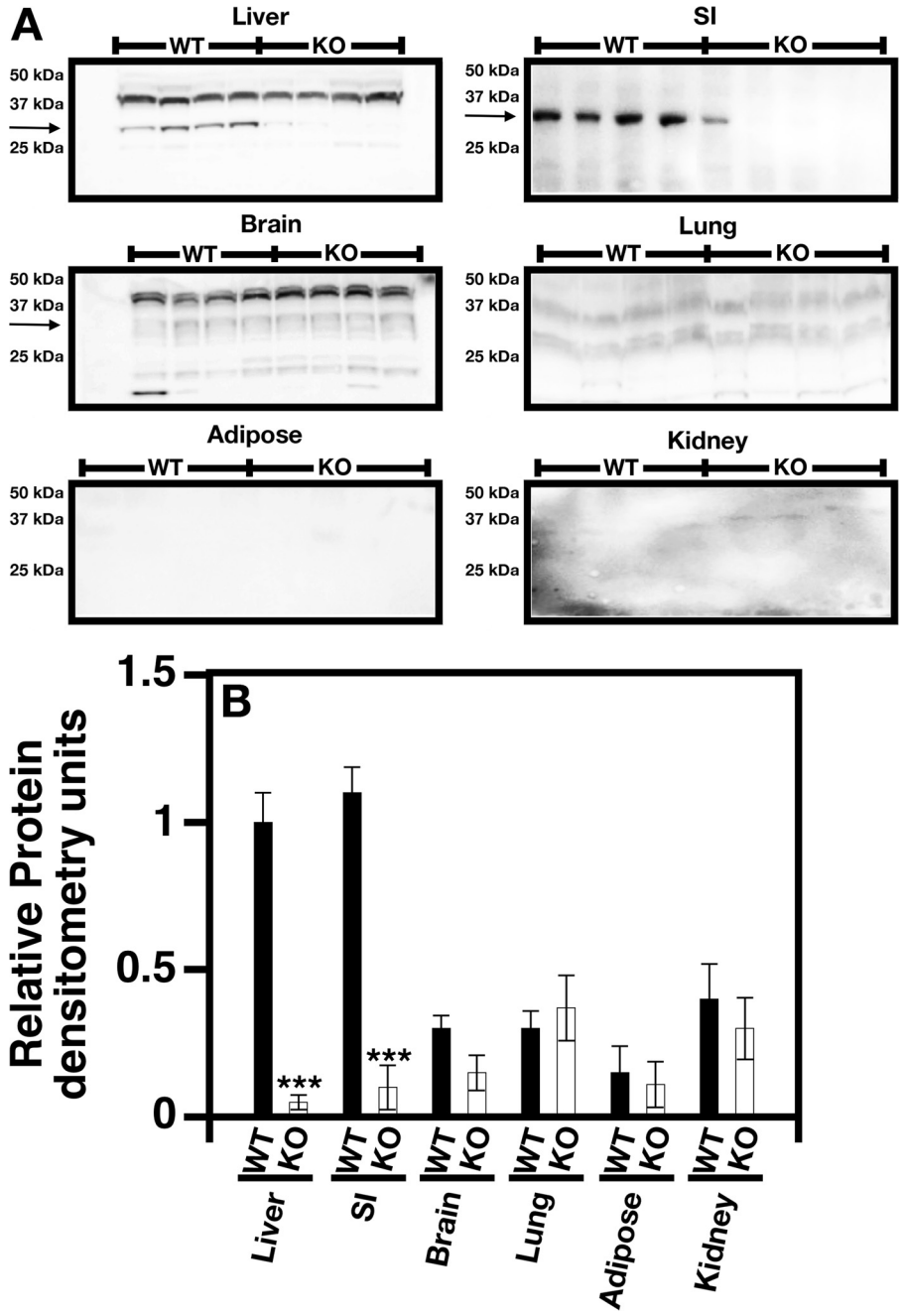

Figure 2. Arv1$^{-/-}$ animals do not express ARV1 protein. Total protein was extracted from the indicated tissues. Proteins were resolved by SDS-PAGE, and ARV1 protein levels were determined by Western blot analysis using anti-ARV1 polyclonal antibodies (Abgent, catalog no. AP10655a). ARV1 protein runs as a 31-kDa protein (*arrow*). Ponceau S staining and the Bradford method were used to load the same amount of protein in each well of all gels (92, 93). WT levels of ARV1 protein density in each tissue were set at a relative value of 1, and ARV1 levels in other tissues were compared with WT. ***, $p < 0.001$. *Error bars*, S.E.

could not detect the protein in brain, lung, adipose, or kidney tissue (Fig. 2*A* and Fig. S1). Densitometry values correlated with band intensities for each organ (Fig. 2*B*).

Thus, *Arv1*$^{-/-}$ animals express a stable truncated *Arv1* mRNA containing exons 1–4, which is not translated into a truncated form of the ARV1 protein. Based on these results, we conclude that *Arv1*$^{-/-}$ mice are devoid of any form of ARV1 protein.

In all of our studies, we tested WT, *Arv1*$^{+/-}$, and *Arv1*$^{-/-}$ animals. We only presented data from *Arv1*$^{+/-}$ animals when they deviated from what we observed for WT animals.

Arv1$^{-/-}$ *mice have a reduced survival rate and display neurological and behavioral deficits*

Lagor and colleagues (23, 24) have reported that *Arv1*$^{-/-}$ whole-body and *nestin-Cre*–mediated NKOs of *Arv1* had reduced survival rates. We tested for this phenotype in our *Arv1*$^{-/-}$ animals by recording survival of a group of 16 males of each genotype beginning at 8 weeks of age until over 20 weeks of age. The first death on the normal chow (NC) was recorded at 12 weeks of age, and by 18 weeks of age, 60% of the *Arv1*$^{-/-}$ animals were dead (Fig. 3, WT (*closed circles*) and KO (*open*

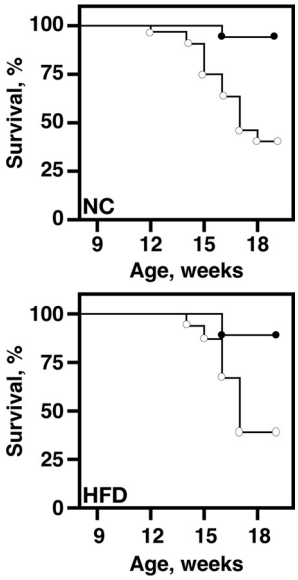

Figure 3. Arv1$^{-/-}$ animals have reduced survival rates. Male WT and *Arv1*$^{-/-}$ animals were fed either NC or an HFD. They were monitored daily, and the age at the time of death was recorded. On the NC, there was a significant difference in survival (log-rank $p = 0.0006$) and also on the HFD (log-rank $p = 0.0202$); $n = 16$. *Closed circles*, WT; *open circles*, *Arv1*$^{-/-}$.

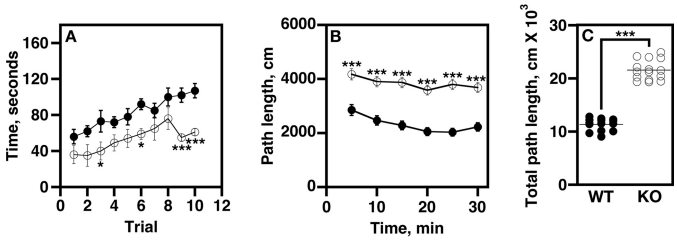

Figure 4. *Arv1*$^{-/-}$ animals display neurological deficits. Male WT and *Arv1*$^{-/-}$ animals were between the ages of 9 and 14 weeks and were individually housed before initiation of the study. Mice were acclimated to the testing room for at least 30 min. *A*, the assay was carried out using EzRod test chambers. For the accelerating rotarod study, mice were given 10 trials with a maximum duration of 3 min with a 30-s intertrial interval. The time of latency to fall was recorded for all trials. *Closed circles*, WT; *open circles*, *Arv1*$^{-/-}$; *B* and *C*, the assay was performed as described under "Experimental procedures." The time and the path length in the center of the open field were determined. Total path length and path length for 30 min at 5-min intervals were determined as measures of locomotor activity. WT, $n = 14$; *Arv1*$^{-/-}$, $n = 15$. *, $p < 0.01$; ***, $p < 0001$. *Error bars*, S.E.

circles)). The survival rate on the high-fat diet (HFD) was similar, with 60% of the mice dead by 17 weeks of age.

During the survival study, we observed that a subset of adult *Arv1*$^{-/-}$ males suffered from seizures. In the case of the *Arv1*$^{-/-}$ males tested, one animal had to be euthanized because of the severity of the event. Palmer *et al.* (24) have also reported that NKO animals suffered seizures.

We next determined whether *Arv1*$^{-/-}$ animals displayed other neurological deficits. We compared the motor coordination between WT and *Arv1*$^{-/-}$ animals using a rotarod test (25). During this test, animals are placed on an accelerated rotating horizontal rod, and the mice must coordinate paw movement to remain on the rod. Ten sequential trials were performed, and latency before the mice fell off of the rod was measured.

WT animals increased their length of time on the rod as the number of trials increased, indicating that they adapted by learning how to remain on the rod. *Arv1*$^{-/-}$ animals fell off the rod sooner than WT animals but had the same increase in time as WT animals (Fig. 4*A*, *trials 3* and *6*, WT (*closed circles*) and KO (*open circles*)), demonstrating an impaired locomotor coordination but retaining some ability to improve performance. However, later trials revealed there was a significant decrease in time on the rod compared with WT animals (Fig. 4*A*, *trials 9* and *10*, WT (*closed circles*) and KO (*open circles*)). Thus, *Arv1*$^{-/-}$ animals display impaired motor coordination.

To complement the rotarod studies, we determined the activity levels of *Arv1*$^{-/-}$ animals using an open field test (26). *Arv1*$^{-/-}$ animals had a higher level of activity than their WT littermates at all time points monitored (Fig. 4*B*, WT (*closed circles*) and KO (*open circles*)). Moreover, the total path length traveled by knockouts was nearly double that of WT animals (Fig. 4*C*, WT (*closed circles*) and KO (*open circles*)).

Finally, we tested for male and female fertility, as it has been noted that *Arv1*$^{-/-}$ mice have lower fertility rates (23). Homozygous male and female *Arv1*$^{-/-}$ mice were mated to Institute of Cancer Research (ICR) mice, and we quantified 1) successful mating by the appearance of a mating plug, 2) the average litter size, and 3) the number of successful litters. ICR mice have been used to examine fertility, as they display excellent reproduction rates (27, 28).

During mating, male mice deposit a mating (copulation/sperm) plug into the female genital tract, which is a gelatinous substance containing lipids and sperm (29). The mating plug solidifies and closes the vaginal tract, which helps in sperm retention. We found that female *Arv1*$^{-/-}$ mice retained mating plugs with a frequency that was similar to their WT littermates (Fig. 5*A*, WT (*black bars*) and KO (*white bars*)). These females had litter sizes that were similar to WT (Fig. 5*B*, WT (*closed circles*) and KO (*open circles*)). Moreover, they produced similar numbers of litters (Fig. 5*C*, WT (*black bars*) and KO (*white bars*)). Male *Arv1*$^{-/-}$ mice were as fertile as their WT littermates under all conditions tested (Fig. 5 (*D–F*), WT (*closed circles* and *black bars*) and KO (*open circles* and *white bars*)). Upon further examination, we found that all pups produced by female *Arv1*$^{-/-}$ animals died within 4 days due to maternal neglect.

Loss of mARV1 reduces high-fat diet–induced obesity

Our *Arv1*$^{-/-}$ mice are maintained on the C57BL/6J mouse background, which is a diet-induced obesity (DIO)-sensitive strain. It has been shown that *Arv1*$^{-/-}$ mice display a lean phenotype (23). To test whether our *Arv1*$^{-/-}$ animals shared this phenotype, we fed them an HFD and determined its effects on weight gain. Animals were fed either NC or an HFD, and body weights were measured weekly for 15 weeks (Fig. 6). When fed an NC diet, both groups of animals more or less maintained their body weight throughout the study (Fig. 7*A*, WT (*closed circles*) and KO (*open circles*)). When fed an HFD, WT mice nearly doubled their body weight over the 15 weeks, whereas *Arv1*$^{-/-}$ mice fed the same diet showed only a slight weight gain that was not statistically significantly different from mutant animals fed NC (Fig. 7*A*, WT (*closed boxes*) and KO (*open boxes*)). WT animals fed an HFD increased their body weight by 160%, whereas the percentage of weight gained for

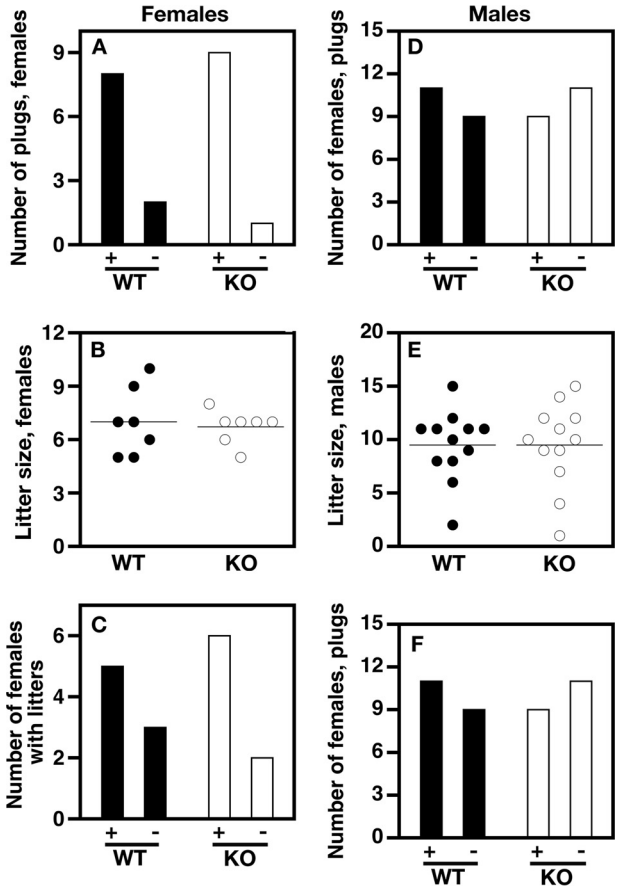

Figure 5. Male and female *Arv1*$^{-/-}$ animals are fertile. *A–C*, sexually mature females (6–7 weeks) were paired with an ICR male (8 weeks). *D–F*, sexually mature males (~3 months) were paired with two ICR females (6 weeks). The presence of a vaginal plug was checked for every day for 6 days, and then the male was removed. Females were checked daily, and size and birth dates of litters were recorded. *A*, *C*, *D*, and *F*, *black bars*, WT; *white bars*, *Arv1*$^{-/-}$; +, success; −, no success. *B* and *E*, *closed circles*, WT; *open circles*, *Arv1*$^{-/-}$.

Arv1$^{-/-}$ mice was minimal. We point out that *Arv1*$^{-/-}$ animals did not lose weight during the entire time of the study whether fed NC or an HFD.

One possibility for this lack of weight gain is that *Arv1*$^{-/-}$ animals consumed less food. Food consumption was determined over a 72-h time period for animals on NC or an HFD. *Arv1*$^{-/-}$ animals consumed more chow, whether on NC or an HFD (Fig. 7*B*, WT (*closed circles*) and KO (*open circles*)). *Arv1*$^{-/-}$ animals fed an HFD consumed ~5 times more food per kg of body weight than their WT littermates (Fig. 7*B*, WT (*closed circles*) and KO (*open circles*)). Thus, *Arv1*$^{-/-}$ animals consume more food but do not gain weight when fed NC or an HFD.

To explore what was the cause of the increased food consumption, we assayed for the levels of several hormones that are known to regulate eating behavior. Ghrelin is secreted by the small intestine and regulates the hunger response by acting as a neuropeptide activating ghrelin receptors in the hypothalamus. There are two forms of ghrelin that differ in acylation status (30). Leptin also regulates hunger and is secreted by adipose tissue, where it functions in the hypothalamus by binding to leptin receptors (31). Leptin acts as an anorexigenic hormone, whereas ghrelin is orexigenic.

Both acylated and deacylated ghrelin levels were increased in 8-week-old *Arv1*$^{-/-}$ animals compared with WT littermates (Fig. 7*C*, *WT* (*closed circles*) and KO (*open circles*)). WT animals secreted high levels of leptin in response to being fed an HFD (7.6 to ~42 ng/ml) (Fig. 7*D*, WT (*closed circles*) and KO, (*open circles*)). In contrast, leptin levels were dramatically decreased in *Arv1*$^{-/-}$ mice, whether they were fed NC or an HFD (Fig. 7*D*, WT (*closed circles*) and KO (*open circles*)). *Arv1*$^{-/-}$ mice fed an HFD secreted ~13-fold less leptin than WT animals.

We next measured adiponectin levels. Adiponectin is an adipocyte-specific adipokine, whose levels correlate with insulin resistance and are reduced in obese individuals (32, 33). *Arv1*$^{-/-}$ animals had elevated adiponectin levels compared with WT mice, whether they consumed NC or an HFD (Fig. 7*E*, WT (*closed circles*) and KO (*open circles*)). *Arv1*$^{-/-}$ animals secreted ~9-fold more adiponectin per total fat mass when fed an HFD (Fig. 7*E*).

Thus, *Arv1*$^{-/-}$ animals have elevated levels of ghrelin and decreased levels of leptin compared with WT animals. These changes may be causing increased food consumption. However, *Arv1*$^{-/-}$ animals have high adiponectin levels that are characteristic of a lean phenotype (34).

A higher metabolic rate could help in maintaining the resistance to diet-induced obesity observed for *Arv1*$^{-/-}$ animals. Several tests were performed to measure metabolic status. Metabolic rate measurements were taken before and after starting an HFD. Measurements were taken every 12 h for 2 days. Before the initiation of the HFD, there were minimal differences in metabolic rates of *Arv1*$^{-/-}$ mice and WT animals (Fig. 8 (*A–C*), WT (*closed circles*) and KO (*open circles*)). However, drastic differences were observed when animals were fed an HFD, as *Arv1*$^{-/-}$ mice had elevated metabolic rates for all parameters tested (Fig. 8 (*A–C*), WT (*closed boxes*) and KO (*open boxes*)). Analysis of the respiratory exchange ratio of both cohorts indicated they metabolized mainly carbohydrate when fed NC, whereas both fats and carbohydrates were used on an HFD (Fig. 8*D*, WT (*closed boxes*) and KO (*open boxes*)).

Thus far, our data strongly suggest that, although *Arv1*$^{-/-}$ animals consume more food due to elevated ghrelin levels and reduced leptin levels, they are resistant to becoming obese, in part due to a higher metabolic rate and increase in energy expenditure.

Blood cholesterol and triglyceride levels are reduced in Arv1$^{-/-}$ *mice*

We next examined whether there were changes in various blood lipid levels due to the lack of diet-induced weight gain. Cholesterol (Chol), triacylglycerides (TAGs), and apolipoprotein levels were determined. *Arv1*$^{-/-}$ mice fed either NC or an HFD had reductions in blood cholesterol levels when compared with WT mice (Fig. 9*A* (NC, 20%; HFD, 60%), WT (*closed circles*), heterozygous (hetero) (*closed diamonds*), and KO (*open circles*)). Heterozygous *Arv1*$^{+/-}$ mice fed an HFD had an increase in cholesterol relative to WT animals when fed an HFD (Fig. 9*A*, WT (*closed circles*); hetero (*closed diamonds*), and KO (*open circles*)). The reason for this observed elevation in blood cholesterol in heterozygotes is unknown. The levels of TAGs observed for animals fed NC were similar for all groups (Fig. 9*B*,

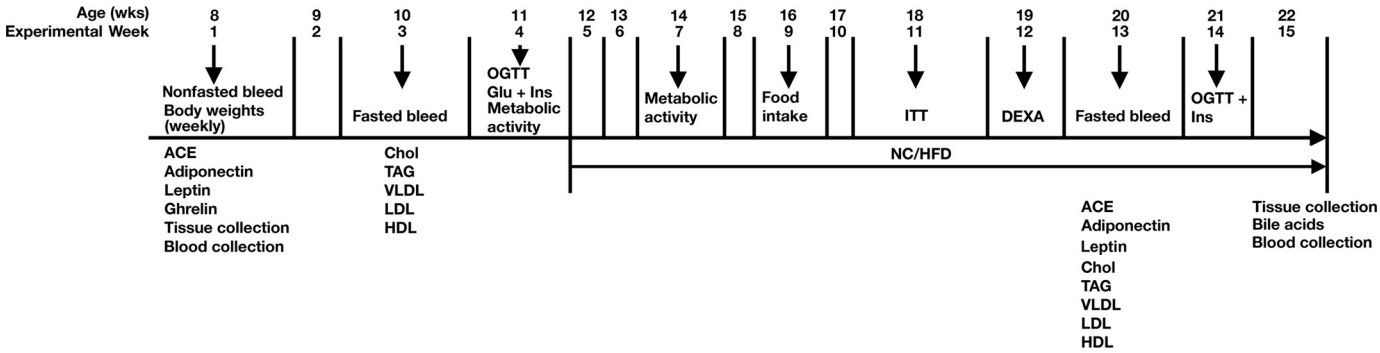

Figure 6. Workflow chart. The diagram indicates the day an experiment was performed and the age of the mice.

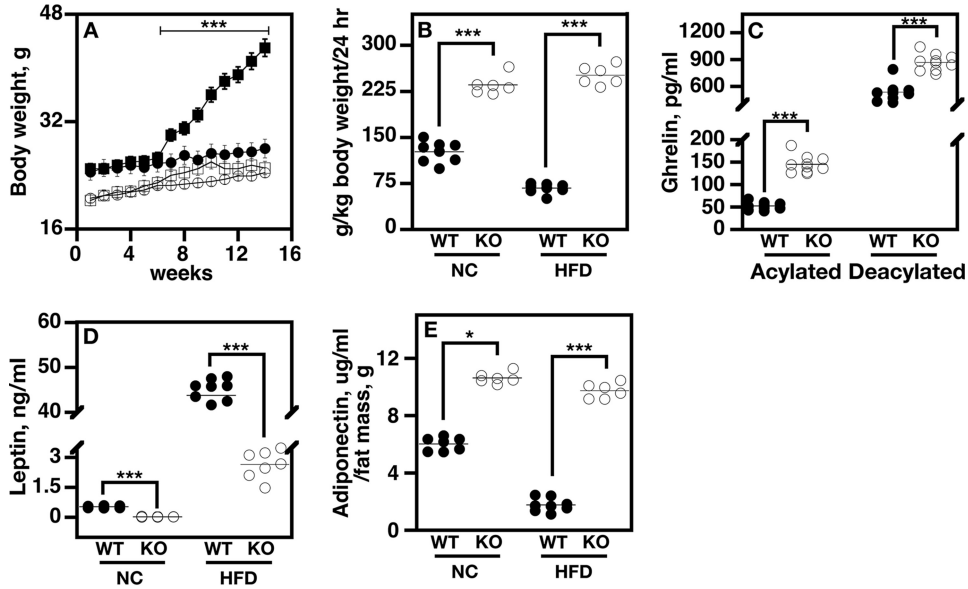

Figure 7. *Arv1*$^{-/-}$ animals are resistant to diet-induced obesity. *A*, body weights of individually housed male *Arv1*$^{-/-}$ and WT mice over 15 weeks, the HFD was added at week 5. *Closed circles*, WT; *open circles*, *Arv1*$^{-/-}$ (NC); *closed boxes*, WT; *open boxes*, *Arv1*$^{-/-}$ (HFD). *B*, the amount of food intake/kg body weight of individually housed male WT and *Arv1*$^{-/-}$ animals were determined over a 24-h period (*closed circles*, WT; *open circles*, *KO*). *C*, acyl and deacyl ghrelin concentrations in plasma were determined in fasted mice (WT (*closed circles*) and *KO* (*open circles*)). *D*, nonfasted leptin concentrations were determined (WT (*closed circles*) and *KO* (*open circles*)). *E*, fasted adiponectin concentrations were determined from serum samples (WT (*closed circles*) and *KO* (*open circles*)). *A* (NC and HFD), WT, $n = 10$; *Arv1*$^{-/-}$, $n = 8$. *B* (NC), WT, $n = 8$; *Arv1*$^{-/-}$, $n = 6$; *B* (HFD), WT, $n = 7$; *Arv1*$^{-/-}$, $n = 6$. *C* (NC), WT, $n = 8$; *Arv1*$^{-/-}$, $n = 10$; HFD, WT, $n = 8$; *Arv1*$^{-/-}$, $n = 10$. *D* (NC), WT, $n = 6$; *Arv1*$^{-/-}$, $n = 5$; D (HFD), WT, $n = 8$; *Arv1*$^{-/-}$, $n = 7$. *E* (NC), WT, $n = 7$; *Arv1*$^{-/-}$, $n = 6$; *E* (HFD), WT, $n = 8$; *Arv1*$^{-/-}$, $n = 6$. *, $p < 0.01$; ***, $p < 0.0001$. *Error bars*, S.E.

WT (*closed circles*); hetero (*closed diamonds*), and KO (*open circles*)). There was a slight trend in reduced levels of TAGs observed in *Arv1*$^{-/-}$ animals. On the other hand, *Arv1*$^{-/-}$ animals on an HFD had a 25% decrease in TAGs compared with WT animals (Fig. 9*B*, WT (*closed circles*), hetero (*closed diamonds*), and KO (*open circles*)). HDL apolipoprotein levels were reduced in *Arv1*$^{-/-}$ animals by 25% (Fig. 9*C*, WT (*closed circles*), *hetero* (*closed diamonds*), and KO (*open circles*)) and 40% (Fig. 9*D*) when fed NC and an HFD, respectively (Fig. 9*C*, WT (*closed circles*), hetero (*closed diamonds*), and KO (*open circles*)). Heterozygous mice had normal HDL levels on NC (Fig. 9*C*, WT (*closed circles*), hetero (*closed diamonds*), and KO (*open circles*)) but elevated levels when fed an HFD (Fig. 9*D*, WT (*closed circles*), hetero (*closed diamonds*), and *KO* (*open circles*)). VLDL and LDL levels were unchanged.

Taken in sum, our data show that loss of ARV1 correlates with reduced blood cholesterol and HDL levels regardless of diet and reduced TAGs levels in animals fed an HFD.

Arv1$^{-/-}$ animals are leaner and have less fat deposition

We used DEXA scanning to analyze total fat and lean mass. *Arv1*$^{-/-}$ animals had a reduced fat mass when compared with WT mice (Fig. 10*A*, WT (*closed circles*) and KO (*open circles*)). The difference was much more pronounced in *Arv1*$^{-/-}$ animals fed an HFD (Fig. 10*A*, WT (*closed circles*) and KO (*open circles*)). HFD-fed *Arv1*$^{-/-}$ animals were leaner than WT mice, but their levels of lean mass were decreased by ~30% (data not shown).

Multiple fat depots were dissected, and fat distribution and mass were determined for animals fed an HFD. The levels of fat mass per gram of body weight in *Arv1*$^{-/-}$ animals were reduced in all fat depots (Fig. 10*B*, WT (*closed circles*) and KO (*open circles*)). Decreases ranged from 3-fold in mesenteric fat to 7.5-fold in epididymal fat. Interestingly, *Arv1*$^{-/-}$ animals contained less brown fat mass and brown fat mass per g of body weight (Fig. 10 (*C* and *D*), WT (*closed circles*) and KO (*open circles*)). Why *Arv1*$^{-/-}$ animals have less brown fat is unknown.

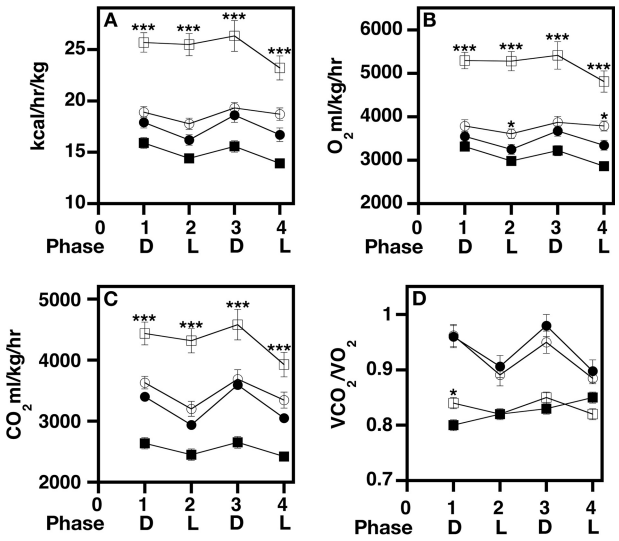

Figure 8. Arv1$^{-/-}$ animals have increased energy expenditure. *A–D*, metabolic studies were performed using the Comprehensive Cage Monitoring System (Columbus Instruments). Parameters were measured for 48 h, beginning and ending at the start of the dark phase of the light cycle. *A*, energy expenditure. *B*, oxygen consumption. *C*, carbon dioxide production. *D*, respiratory exchange ratio. All statistical data were calculated as described under "Experimental procedures." For NC, WT (*closed circles*) and *Arv1*$^{-/-}$ (*open circles*) are shown; for HFD, WT (*closed boxes*) and *Arv1*$^{-/-}$ (*open boxes*) are shown. For WT, $n = 8$; for *Arv1*$^{-/-}$, $n = 6$. *, $p < 0.01$; ***, $p < 0.0001$. *Error bars*, S.E.

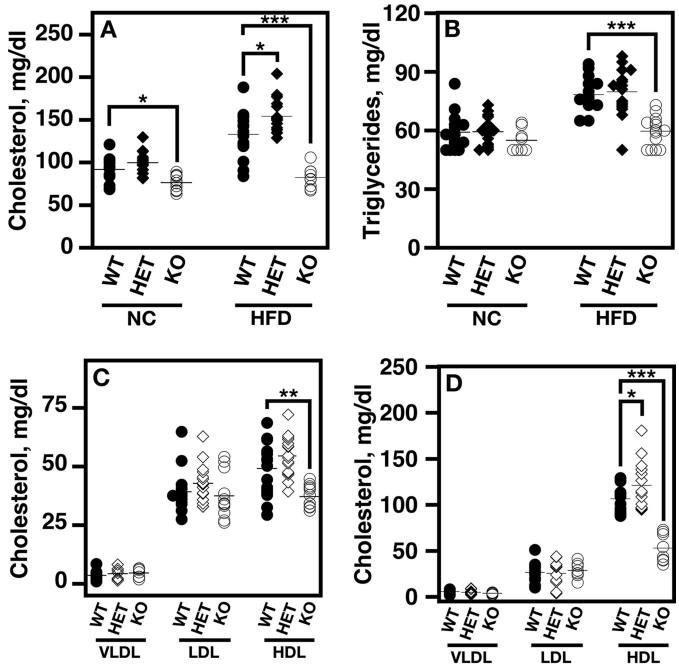

Figure 9. Arv1$^{-/-}$ animals have reduced blood cholesterol and triglyceride levels. Cholesterol, triglycerides, and blood apolipoprotein levels were determined for animals on the NC the third week of the study and again after 8 weeks on an HFD. *A*, serum cholesterol levels in mice were measured after an overnight fast. Cholesterol concentrations were determined enzymatically from serum (Thermo DMA, Arlington, TX). *B*, serum triglyceride levels were also measured after an overnight fast. Whole blood was collected, and triglycerides were assessed on a hand-held meter (CardioChek). *C* and *D*, apolipoprotein levels. The LipoPrint LDL system was used for calculations according to the manufacturer's instructions. *Closed circles*, WT; *closed triangles*, hetero; *Arv1*$^{+/-}$; *open circles, Arv1*$^{-/-}$. *A* (NC), WT, $n = 16$; *Arv1*$^{+/-}$, $n = 16$; *Arv1*$^{-/-}$, $n = 12$; *A* (HFD), WT, $n = 15$; *Arv1*$^{+/-}$, $n = 16$; *Arv1*$^{-/-}$, $n = 9$ (cholesterol). *B* (NC), WT, $n = 16$; *Arv1*$^{+/-}$, $n = 16$; *Arv1*$^{-/-}$, $n = 8$; *B* (HFD), WT, $n = 16$; *Arv1*$^{+/-}$, $n = 16$; *Arv1*$^{-/-}$, $n = 14$ (triglyceride). *C* (NC), WT, $n = 12$; *Arv1*$^{+/-}$, $n = 7$; *Arv1*$^{-/-}$, $n = 7$ (VLDL). *C* (NC), WT, $n = 15$; *Arv1*$^{+/-}$, $n = 16$; *Arv1*$^{-/-}$, $n = 12$ (LDL). C (NC), WT, $n = 16$; *Arv1*$^{+/-}$, $n = 16$; *Arv1*$^{-/-}$, $n = 12$ (HDL). *D* (HFD), WT, $n = 12$; *Arv1*$^{+/-}$, $n = 12$; *Arv1*$^{-/-}$, $n = 8$ (VLDL). *D* (HFD), WT, $n = 15$; *Arv1*$^{+/-}$, $n = 14$; *Arv1*$^{-/-}$, $n = 8$ (LDL). *D* (HFD), WT, $n = 15$; *Arv1*$^{+/-}$, $n = 15$; *Arv1*$^{-/-}$, $n = 8$ (HDL). *, $p < 0.01$; **, $p < 0.001$; ***, $p < 0.0001$. *Error bars*, S.E.

They do display higher metabolic rates then WT animals and are unable to gain weight on an HFD.

Arv1$^{-/-}$ *mice are more glucose-tolerant and have increased insulin sensitivity*

The C57BL/6J mouse strain is used as a model for examining how obesity affects the onset of diabetes (35, 36). As our *Arv1*$^{-/-}$ animals showed resistance to diet-induced obesity, we looked at whether there was a correlation between lack of weight gain and reduced signs of prediabetes.

We first performed an oral glucose tolerance test (OGTT) to see whether changes in diet affected glucose tolerance. Glucose excursion rates were similar between WT and *Arv1*$^{-/-}$ animals fed NC (Fig. 11*A*, WT (*closed circles*) and KO (*open circles*)). However, *Arv1*$^{-/-}$ animals had significant decreases in fasting blood glucose levels (Fig. 11*B*, WT (*closed circles*) and KO (*open circles*); NC). Moreover, *Arv1*$^{-/-}$ animals fed an HFD had increased glucose excursion rates (Fig. 11*A*, WT (*closed boxes*) and KO (*open boxes*)) and lower fasting blood glucose levels than WT animals (Fig. 11*B*, WT (*closed circles*) and KO (*open circles*); HFD). HFD ending blood glucose levels in *Arv1*$^{-/-}$ animals returned to levels that were seen before the initiation of the study, whereas *WT* levels remained high (Fig. 11*A*, WT (*closed boxes*) and KO (*open boxes*); 0 *versus* 120 min time points). The fact that WT mice fed an HFD had elevated blood glucose levels at the end of the OGTT further validates the glucose intolerance phenotype associated with the DIO model (36). The data also indicate that *Arv1*$^{-}$/$^{-}$ animals are resistant to becoming glucose-intolerant when fed an HFD.

We determined insulin secretion during the OGTT. Insulin levels in WT and *Arv1*$^{-/-}$ animals fed NC peaked coincident with glucose levels (first-phase insulin response) and decreased thereafter (Fig. 11*C*, WT (*closed circles*) and KO (*open circles*)). However, *Arv1*$^{-/-}$ animals secreted less insulin than did WT mice (Fig. 11*C*, WT (*closed circles*) and KO (*open circles*)) and had lower baseline fasting insulin levels (Fig. 11*D*, WT (*closed circles*) and KO (*open circles*)).

When fed an HFD, WT mice secreted higher levels of insulin during the first-phase insulin response compared with WT animals fed NC (~9 ng/ml *versus* 2.2 ng/ml) (Fig. 11*C*, *closed boxes versus open boxes*). On the other hand, *Arv1*$^{-/-}$ animals fed an HFD secreted drastically less insulin than WT animals (Fig. 11*C*, WT (*closed boxes*) and KO (*open* boxes)), with levels being equivalent to those observed on NC (Fig. 11*C*, 1.3 ng/ml *versus* 0.9 ng/ml). Overall, there was ~9-fold reduction in first-phase insulin response secretion in *Arv1*$^{-/-}$ animals compared with WT animals fed an HFD (Fig. 11*C*). The fasting insulin levels of *Arv1*$^{-/-}$ animals fed an HFD were again reduced compared with WT animals (Fig. 11*D*, WT (*closed circles*) and KO (*open circles*) (2.8 pg/ml *versus* 0.25 pg/ml)).

Finally, an insulin tolerance test was performed on animals fed NC or an HFD. WT and *Arv1*$^{-/-}$ animals responded with normal sensitivity to the low insulin dose (0.5 units/kg) with a

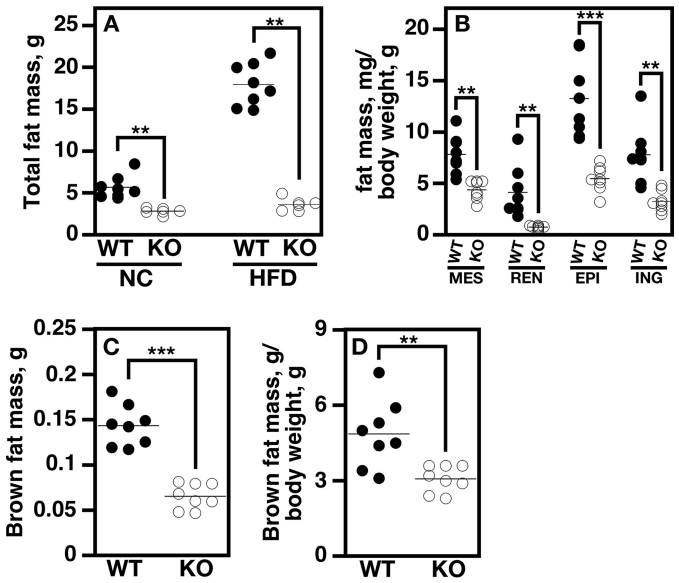

Figure 10. *Arv1*$^{-/-}$ animals remain lean on a high-fat diet. DEXA and dissected fat pads were used to measure adiposity in NC- and HFD-fed male mice. *A*, total fat mass. Values represent the sum of all fat depots. *B*, adipose tissue dissections were performed on an NC-fed group of mice ~10 weeks of age. Adipose tissue was dissected from the inguinal fat pad (subcutaneous fat), epididymal, renal (retroperitoneal), and mesenteric fat pads (visceral fat). Individual values were then divided by weight of an animal at the time of dissection. Values are represented as mg of fat mass/g of weight. *C* and *D*, total brown adipose tissue was dissected from the suprascapular area of the back from an NC-fed group of mice ~10 weeks of age. Total brown fat mass was calculated by weighing the tissue extracted. Total brown adipose mass/g of tissue was calculated by dividing total brown adipose mass by weight. *A* (NC), WT, $n = 7$; *Arv1*$^{-/-}$, $n = 6$; *A* (HFD), WT, $n = 8$; *Arv1*$^{-/-}$, $n = 6$. *B*, WT, $n = 7$; *Arv1*$^{-/-}$, $n = 8$ (MES). *B* (REN), WT, $n = 7$; *Arv1*$^{-/-}$, $n = 10$. *B* (EPI), WT, $n = 6$; *Arv1*$^{-/-}$, $n = 7$. *B* (ING), WT, $n = 7$; *Arv1*$^{-/-}$, $n = 7$. *C*, WT, $n = 8$; *Arv1*$^{-/-}$, $n = 8$. *D*, WT, $n = 8$; *Arv1*$^{-/-}$, $n = 8$). **, $p < 0.001$; ***, $p < 0.0001$. *Error bars*, S.E.

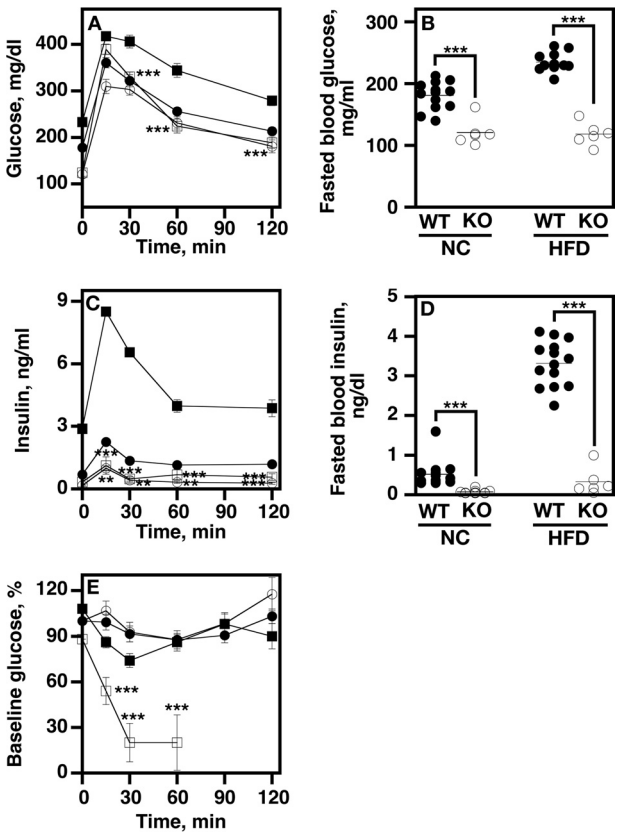

Figure 11. Arv1$^{-/-}$ animals fed a high-fat diet remain glucose-tolerant and insulin-sensitive. *A*, male mice were subjected to an OGTT following 9 weeks on an HFD, or age-matched mice were fed an NC. *A* and *B*, mice were fasted for 16 h before initiation of the study. *C* and *D*, male mice that were subjected to an OGTT test before and after HFD feeding were used for determining insulin levels. Basal insulin levels were determined in mice fasted for 16 h. Insulin levels measured during the OGTT are presented in *A* and *B*. *E*, mice were fasted for 4 h. NC-fed animals were given 0.5 units/kg of insulin by intraperitoneal injection. HFD-fed animals were given 1.0 unit/kg of insulin by intraperitoneal injection. At the indicated times, blood glucose values were obtained. *A*, *C*, and *E* (NC), WT (*closed circles*) and *Arv1*$^{-/-}$ (*open circles*). *A*, *C*, and *E* (HFD), WT (*closed boxes*) and *Arv1*$^{-/-}$ (*open boxes*). *B* and *D*, WT (*closed circles*) and *Arv1*$^{-/-}$ (*open circles*). *A*, *C*, and *E* (NC), WT, $n = 12$; *Arv1*$^{-/-}$, $n = 6$. *A*, *C*, and *E* (HFD), WT, $n = 11$; *Arv1*$^{-/-}$, $n = 6$. *B* (NC), WT, $n = 12$; *Arv1*$^{-/-}$, $n = 6$. *B* (HFD), WT, $n = 11$; *Arv1*$^{-/-}$, $n = 6$. *D* (NC), WT, $n = 10$; *Arv1*$^{-/-}$, $n = 8$. *D* (HFD), WT, $n = 14$; *Arv1*$^{-/-}$, $n = 6$. **, $p < 0.001$; ***, $p < 0.0001$. *Error bars*, S.E.

small decrease in blood glucose levels (Fig. 11*E*, WT (*closed circles*) and KO (*open circles*)). WT animals fed an HFD also had a reduction in glucose levels using a much higher insulin dose (1 unit/kg) and recovered as seen by an increase in their glucose levels (Fig. 11*E*, WT (*closed boxes*)). On the other hand, *Arv1*$^{-/-}$ animals fed an HFD were still highly insulin-sensitive, requiring glucose supplementation by 60 min, at which time they were removed from the study (Fig. 11*E*, *KO* (*open boxes*)).

Arv1$^{-/-}$ *mice have reduced signs of NAFLD*

Insulin resistance is tightly associated with the appearance of NAFLD and leads to the induction of lipogenesis in the liver (10). Accumulation of liver TAGs, cholesterol, and fatty acids contributes to, or is the reason for, the onset of fatty liver (37–39). Because our *Arv1*$^{-/-}$ animals remained insulin-sensitive when fed an HFD, we explored whether the insulin sensitivity phenotype correlated with reduced signs of NAFLD.

We first assayed for the rate of lipogenesis in the livers of animals fed a Western diet by measuring the levels of TAGs, cholesterol, LDL, HDL, and free fatty acids (FFAs). *Arv1*$^{-/-}$ animals had reduced lipid levels compared with WT animals (Fig. 12 (*A* and *B*), TAGs (8-fold); Chol (5-fold); LDL (5-fold); HDL (6-fold); FFAs (8-fold); WT (*closed circles*); *KO* (*open circles*)).

Visualization of the gross morphology of livers from WT animals revealed that they were enlarged and had a pale color consistent with a high fat content (Fig. 12*C*). *Arv1*$^{-/-}$ livers were normal in size and deep pink in color (Fig. 12*C*). Histological staining of WT livers indicated the presence of micro- and macrosteatosis, hepatocyte ballooning, and the presence of Mallory bodies (Fig. 12*D*, *arrow*, *portal vein*). WT livers had a standard inflammation grade of 3 and a fibrotic stage of 1 ($n = 6$) (40). *Arv1*$^{-/-}$ livers displayed reduced histological signs of hepatic steatosis, and all had a standard inflammation grade of 2 and a fibrotic stage of 0 ($n = 6$).

Finally, we examined hepatic TAG export to begin to understand the physiology underlying the reduction of lipid production and attenuation of NAFLD. Animals were challenged with a bolus of olive oil in the presence of Pluronic F127, an endothelial lipase inhibitor, and blood TAGs levels were determined at the indicated times. *Arv1*$^{-/-}$ animals had a significant decrease in TAG production compared with WT animals (Fig. 12*E*, WT (*closed circles*) and *KO* (*open circles*)).

Finally, serum clinical chemistries were analyzed on HFD-fed animals. Alkaline phosphatase levels were increased in

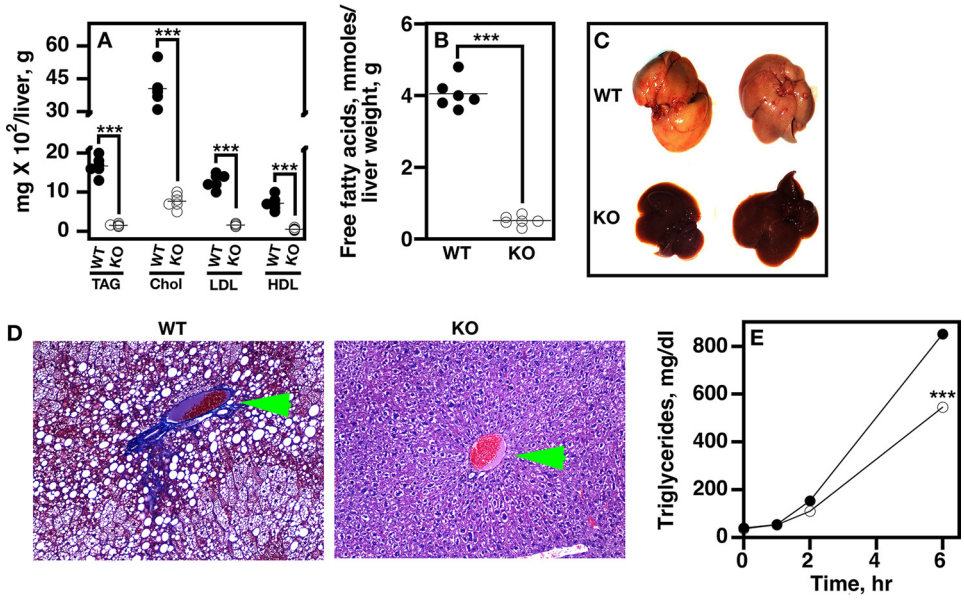

Figure 12. Arv1$^{-/-}$ animals fed a high-fat diet have reduced signs of NAFLD. Liver tissue was extracted from euthanized animals using standard sterile surgical techniques. *A* and *B*, lipid levels were determined using standard commercial assay kits and calculated per g of liver. *C*, WT and *Arv1*$^{-/-}$ animal livers. *D*, tissues were embedded in paraffin blocks and cut on 4 μm. H&E-processed tissues were examined using a Nikon Eclipse 50i clinical microscope. The chronic hepatitis assessment scheme was the Scheuer Classification for Grading and Staging of Chronic Hepatitis (95). The *green arrows* in *panels* in *D* indicate the portal vein. *E*, mice were fasted for 4 h. Hepatic triglyceride export was measured in NC-fed 10-week-old WT and *Arv1*$^{-/-}$ mice measured following intraperitoneal Pluronic F-127 injection (500 mg/kg). *A*, *B*, and *E*, WT (*closed circles*) and *Arv1*$^{-/-}$ (*open circles*). *A* (triglyceride), WT, $n = 5$; *Arv1*$^{-/-}$, $n = 5$. *A* (cholesterol), WT, $n = 5$; *Arv1*$^{-/-}$, $n = 6$. *A* (LDL), WT, $n = 6$; *Arv1*$^{-/-}$, $n = 6$. *A* (HDL), WT, $n = 6$; *Arv1*$^{-/-}$, $n = 6$. *B*, WT, $n = 6$; *Arv1*$^{-/-}$, $n = 6$. ***, $p < 0.0001$. *Error bars*, S.E.

Arv1$^{-/-}$ mice (WT = 85.50 ± 5.74 IU/liter *versus* KO = 262.00 ± 17.09 IU/liter, $p < 0.001$), suggesting an altered hepatobiliary function. Blood urea nitrogen was also elevated (WT = 19.00 ± 0.91 mg/dl *versus* KO = 26.75 ± 1.65 mg/dl, $p < 0.001$). Typically, lactate dehydrogenase is elevated in animals fed an HFD, which is consistent with WT animal measurements (886.63 ± 127.61 IU/liter).[4] The lactate dehydrogenase levels in *Arv1*$^{-/-}$ animals were lower than that seen in NC-fed male C57BL/6 mice (483.50 ± 98.18 IU/liter). Alanine aminotransferase, aspartate aminotransferase, and γ-glutamyl transferase levels in *Arv1*$^{-/-}$ animals were similar to values observed for WT animals.

Arv1$^{-/-}$ *mice accumulate stearic acid and have decreased stearoyl-CoA desaturase 1 (SCD1) expression in the liver*

Total free fatty acid levels were reduced in the livers of *Arv1*$^{-/-}$ animals. Thus, we determined the fatty acid composition of *Arv1*$^{-/-}$ livers using GC/MS. *Arv1*$^{-/-}$ animals accumulated stearic acid (18:0) and arachidonic acid (20:0) and had reduced levels of oleic acid (18:1Δ9), whether fed NC or an HFD (Fig. 13 (*A* and *B*), WT (*closed circles*) and *KO* (*open circles*)).

Stearic acid is the precursor for the synthesis of oleic acid and is a substrate for SCD1. SCD1 activity is the rate-limiting step in the production of oleic acid by adding a double bond to stearic acid, which leads to the production of monounsaturated fatty acids.

As SCD1 activity modulates the level of stearic acid, we determined its mRNA expression and protein levels. *SCD1* mRNA expression was drastically reduced in *Arv1*$^{-/-}$ animals compared with WT animals (data not shown). The reduction in

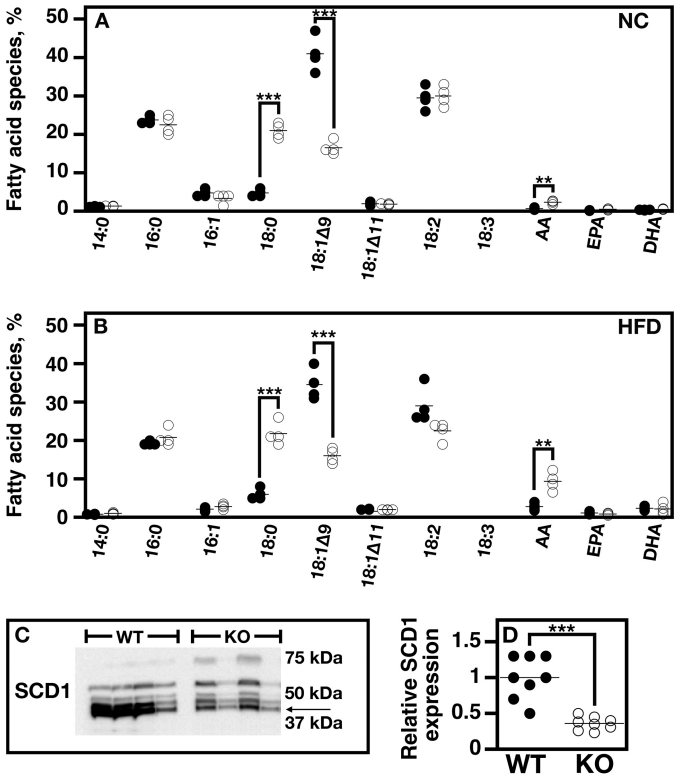

Figure 13. Arv1$^{-/-}$ animals have reduced levels of oleic acid and reduced SCD1 activity in the liver. Animals were either fed NC or an HFD. *A*, fatty-acid levels in the livers of animals fed NC. *B*, fatty acid levels in the livers of animals fed HFD. *C*, SCD1 protein levels. *D*, densitometry of *C*. Protein identification was determined using anti-SCD1 polyclonal antibodies. Ponceau S staining and the Bradford method were used to load the same amount of protein in each well (92, 93). *A* and *B*, WT (*closed circles*) and *Arv1*$^{-/-}$ (*open circles*). *D*, WT (*closed circles*) and *KO* (*open circles*); WT, $n = 6$; *Arv1*$^{-/-}$, $n = 6$. **, $p < 0.001$; ***, $p < 0.0001$ ($n = 8$). *Error bars*, S.E.

[4] M. Hayward, personal communication.

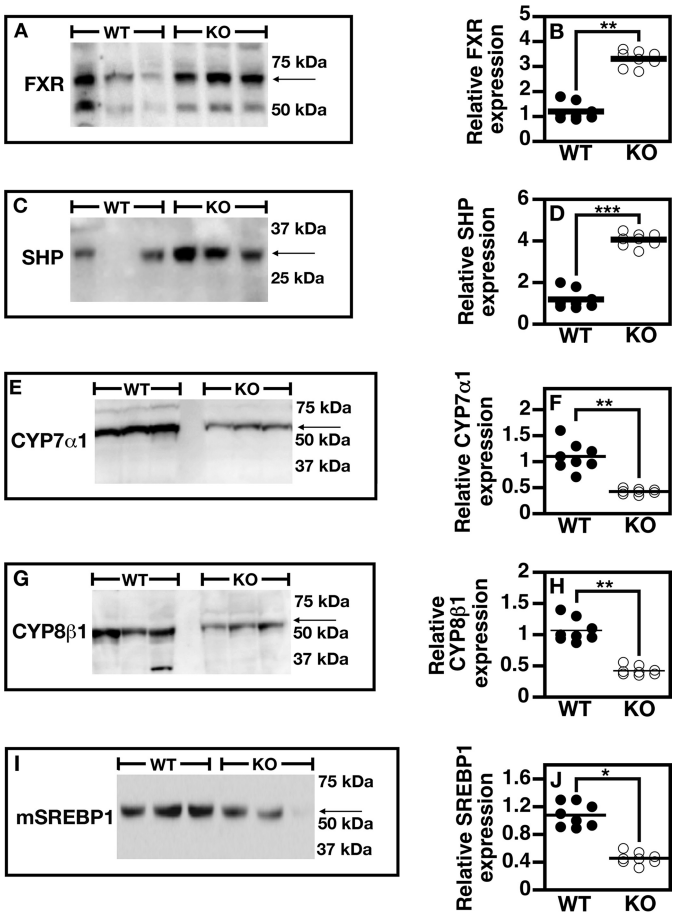

Figure 14. FXR signaling is activated in the livers of *Arv1*$^{-/-}$ animals. WT and *Arv1*$^{-/-}$ animals were fed an HFD. At the end of the study, total protein was extracted and was resolved by SDS-PAGE (*A*, *C*, *E*, *G*, and *I*). Protein identification was determined by Western blot analysis using polyclonal antibodies against the indicated proteins. Ponceau S staining and the Bradford method were used to load the same amount of protein in each well (92, 93). Protein levels were determined using densitometry. *B*, *D*, *F*, *H*, and *J*, WT (*closed circles*) and *Arv1*$^{-/-}$ (*open circles*). *, $p < 0.01$; **, $p < 0.001$; ***, $p < 0.0001$ ($n = 8$).

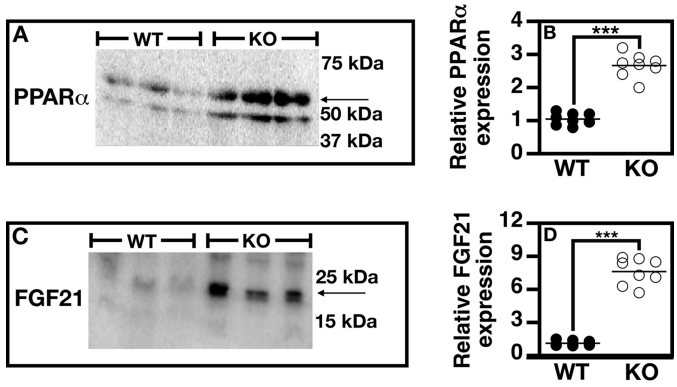

Figure 15. PPARα signaling is activated in the livers of *Arv1*$^{-/-}$ animals. WT and *Arv1*$^{-/-}$ animals were fed an HFD. At the end of the study, total protein was extracted and was resolved by SDS-PAGE (*A* and *C*). Protein identification was determined by Western blot analysis using anti-FXR and anti-SHP polyclonal antibodies. Ponceau S staining and the Bradford method were used to load the same amount of protein in each well (92, 93). Protein levels were determined using densitometry. *B* and *D*, WT (*closed circles*) and *Arv1*$^{-/-}$ (*open circles*). *, $p < 0.01$ ($n = 8$).

mRNA expression directly correlated with reduced SCD1 protein level (Fig. 13 (*C* and *D*), WT (*closed circles*) and *KO* (*open circles*), and Fig. S2).

Farnesol X receptor (FXR) protein levels are increased in the livers of Arv1$^{-/-}$ *mice*

It was shown previously that mice treated with ASOs to *ARV1* showed signs of liver FXR signaling activation (20). FXR signaling results in both an inhibition of sterol response element-binding protein 1c (SREBP1-c)-dependent transcription and maturation, leading to reductions in the expressions of *FAS* (fatty acid synthase) and *ACC1* (acetyl-CoA carboxylase), and activation of peroxisome proliferator-activating receptor α (PPARα)-dependent signaling, resulting in increases in fibroblast growth factor 21 (FGF21) levels and fatty acid β-oxidation.

Based on these previous results, we examined the status of FXR signaling in the livers of *Arv1*$^{-/-}$ animals. We first measured the protein levels of FXR and its downstream target, small heterodimer protein (SHP). FXR protein levels were induced (Fig. 14 (*A* and *B*), WT (*closed circles*) and *KO* (*open circles*); Fig. S3), and this correlated with a concomitant increase in SHP (Fig. 14 (*C* and *D*), WT (*closed circles*) and *KO* (*open circles*), and Fig. S3). These increases were not seen in WT animals.

We next examined the levels of the SHP downstream targets, CYP7α1 and CYP8β1. Both CYP7α1 and CYP8β1 are required for the synthesis of bile acids, and their expressions are reduced upon FXR activation. We found that the protein levels of both CYP7α1 and CYP8β1 were reduced in the livers of *Arv1*$^{-/-}$ animals when compared with those levels seen in WT livers (Fig. 14 (*E–H*), WT (*closed circles*) and *KO* (*open circles*), and Fig. S4). Moreover, mature SREBP1 protein levels were reduced (Fig. 14 (*I* and *J*), WT (*closed circles*) and *KO* (*open circles*), and Fig. S4).

PPARα levels are elevated in the livers of Arv1$^{-/-}$ *mice*

We next looked at the status of PPARα signaling by determining FGF21 protein levels. *Arv1*$^{-/-}$ animals displayed increases in PPARα (Fig. 15 (*A* and *B*), WT (*closed circles*) and *KO* (*open circles*), and Fig. S5) and FGF21 (Fig. 15 (*C* and *D*), WT (*closed circles*) and *KO* (*open circles*), and Fig. S5) protein levels, when compared with levels seen in WT animals.

Overall, our results strongly suggest that liver FXR and PPARα signaling pathways are activated in *Arv1*$^{-/-}$ animals, with activation probably contributing to a reduction in liver lipogenesis and reduced signs of NAFLD.

Arv1$^{-/-}$ *mice have an altered bile acid composition in the SI*

Liver cholesterol is a substrate for bile acid synthesis. Bile acids are secreted into the SI for fecal excretion and/or reabsorbed by the portal circulatory system. Any changes in the flux of bile acid transport and/or metabolism could affect liver cholesterol homeostasis. We found that the CYP7α1 and CYP8β1 enzymes required for the synthesis of bile acids were downregulated. It is feasible that this may cause defects in bile acid composition in *Arv1*$^{-/-}$ animals. Thus, we used GC/MS to determine the intestinal bile acid composition of *Arv1*$^{-/-}$ animals.

We first determined the lipid content in the feces to determine whether there were global changes in overall lipid levels.

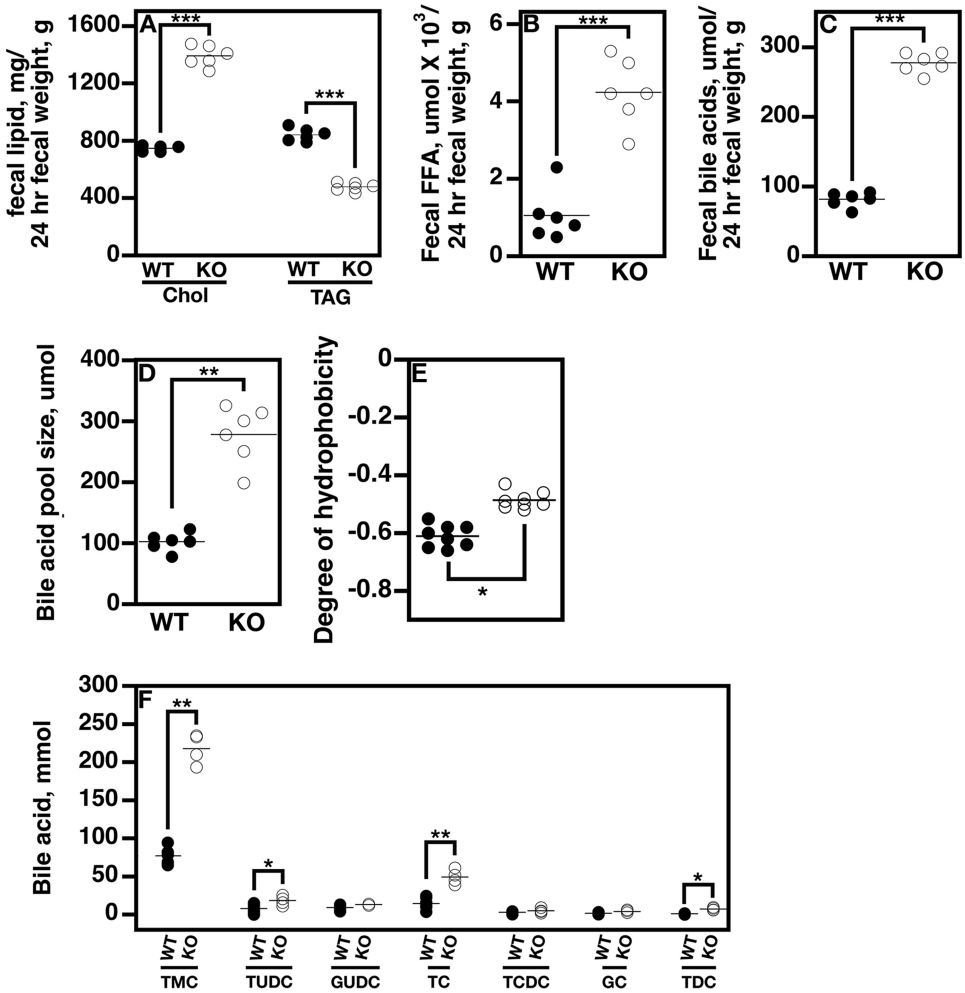

Figure 16. Arv1$^{-/-}$ animals have elevated fecal lipid levels and an altered bile acid intermediate composition. *A–C*, fecal lipids were extracted from male animals using hexane/2-propanol (3:2) (94). Lipid levels were determined using commercially available assay kits. *D–F*, total bile acid pools and compositions in intestines were determined using a previously published protocol (41). *A–D*, WT (*closed circles*) and *Arv1*$^{-/-}$ (*open circles*). *A–E*, WT, $n = 6$; *Arv1*$^{-/-}$, $n = 6$. *F*, WT, $n = 4$; *Arv1*$^{-/-}$, $n = 4$. *, $p < 0.01$; **, $p < 0.001$; ***, $p < 0.0001$.

Arv1$^{-/-}$ animals had increased levels of fecal cholesterol, fatty acids, and total bile acids compared with WT animals (Fig. 16 (*A–C*), WT (*closed circles*) and *KO* (*open circles*)). Analysis of bile acid composition in the SI showed that knockouts had a larger bile acid pool (Fig. 16*D*, WT (*closed circles*) and *KO* (*open circles*)) that was more hydrophobic (Fig. 16*E*, WT (*closed circles*) and *KO* (*open circles*)). Changes were observed in the levels of tauromuricholic acid (TMC), tauroursodeoxycholic acid (TUDC), taurocholic acid (TC), and taurodeoxycholic acid (TDC) (Fig. 16*F*).

The levels of intestinal FXR are induced, but this does not lead to increased SHP protein

TMC is a known antagonist of FXR signaling. Thus, we asked whether there was a relationship between TMC accumulation and decreased FXR effects in the SI of *Arv1*$^{-/-}$ animals. Interestingly, FXR protein levels were induced when compared with WT animals (Fig. 17 (*A* and *B*), WT (*closed circles*) and *KO* (*open circles*), and Fig. S6). However, FXR accumulation did not result in the accumulation of SHP (Fig. 17 (*C* and *D*), WT (*closed circles*) and *KO* (*open circles*), and Fig. S6).

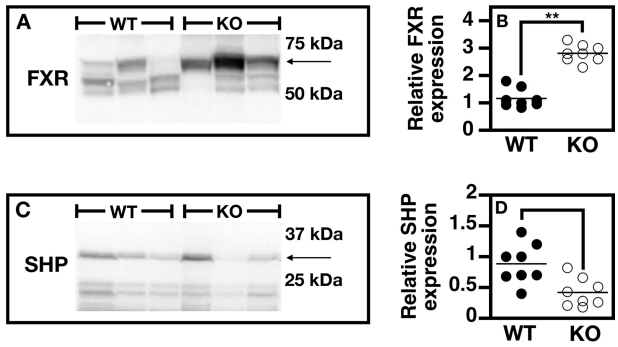

Figure 17. FXR signaling is not activated in the small intestines of *Arv1*$^{-/-}$ animals. WT and *Arv1*$^{-/-}$ animals were fed an HFD. At the end of the study, total protein was extracted and resolved by SDS-PAGE (*A* and *C*). Protein identification was determined by Western blot analysis using anti-FXR and anti-SHP polyclonal antibodies. Ponceau S staining and the Bradford method were used to load equivalent amounts of protein in each well (92, 93). Protein levels were determined using densitometry. *B* and *D*, WT (*closed circles*) and *Arv1*$^{-/-}$ (*open circles*). *, $p < 0.01$ ($n = 8$).

Discussion

Arv1$^{-/-}$ animals fed an HFD 1) were resistant to diet-induced obesity (although they (i) consumed more chow, (ii) had higher levels of ghrelin, and (iii) had lower levels of leptin), 2)

had increased energy expenditure, 3) had reduced levels of blood cholesterol and TAGs, 4) retained glucose tolerance and insulin sensitivity, 5) had reduced fat deposition in several fat depots, 6) had reduced levels of liver cholesterol, TAGs, and fatty acids, 7) excreted high levels of fecal cholesterol, TAGs, bile acids, and fatty acids, 8) had an altered bile acid composition in the SI and accumulated the FXR antagonist, TMC, 9) showed signs of activated FXR and PPARα signaling in the liver and lack of FXR signaling in the SI, and 10) showed few signs of NAFLD. Our results strongly suggest that complete loss of *Arv1* protects mice from acquiring MetS and NAFLD in response to an HFD challenge. Although the function of ARV1 is still up for debate (13–15, 17–19), evidence is accumulating that suggests its involvement in maintaining proper sterol distribution (16, 20, 42, 43). As was shown previously (23, 24), our $Arv1^{-/-}$ animals had reduced survival rates and suffered from seizures, which occasionally resulted in animals being euthanized. In addition to impaired locomotor coordination, $Arv1^{-/-}$ mice were more active than WT mice in an open field, suggesting a generalized neurological defect. Finally, we found no fertility defects, although pups born to $Arv1^{-/-}$ females all died due to maternal neglect.

Genetic linkage studies have associated SNPs in the *hARV1* locus with prostate cancer (44), whereas other SNPs have been identified in searches for loci regulating 1) low-density apolipoprotein– cholesterol and ApoB levels (45), 2) obesity, 3) diabetes, 4) plasma HDL levels, 5) body weight, 6) blood pressure, and 7) fat response to dietary restriction. It is interesting that several of these parameters are perturbed in $Arv1^{-/-}$ animals.

There is also a neurological link between specific mutations in the coding sequence of *ARV1* and epileptic encephalopathy (24, 46). The mutations identified result in a single amino acid change (Q189R), or a nearly complete deletion of the ARV1 homology domain (Lys^{59}–Asn^{98}) (24, 46). MRI brain imaging of infants with this disorder shows the appearance of brainstem lesions (24). Mouse model studies using a neuronal knockout of *mARV1* found that these mice suffered from seizures and had reduced survival rates (24). Our preliminary histology results looking at brain sections of WT and $Arv1^{-/-}$ animals post-HFD revealed no differences in gross morphology (white and gray matter) and neuron numbers.[5] As loss of *ARV1* has now been linked to several disease states, it will be important to uncover the exact molecular function of ARV1 and how this relates to the regulation of lipid homeostasis, neurological function, and possibly cancer progression.

The lack of weight gain of $Arv1^{-/-}$ animals fed an HFD is highly interesting in light of increased food consumption, elevated levels of ghrelin, and lower levels of leptin. The opposite correlation has been seen in obese individuals, where leptin levels are increased and ghrelin levels decreased (32, 33). These individuals are considered leptin-resistant (47). Obesity has also been associated with reduced adiponectin secretion (48). Our $Arv1^{-/-}$ animals secreted more adiponectin per gram of fat mass and had a higher adiponectin/leptin ratio (~9:1) than WT animals. A high ratio seems to be critical for establishing good "metabolic" health (49); an adiponectin/leptin ratio > 1.0 is considered advantageous. Adiponectin activates PPARα signaling through binding to the adiponectin receptor, AdipoR2 (50). FXR signaling also activates PPARα. PPARα activation increases FGF21 levels. FGF21 improves energy production by increasing the utilization of fatty acids (51) and is a potent inhibitor of hepatic steatosis (52). Our results showed that FGF21 levels were elevated in $Arv1^{-/-}$ animals. Thus, FGF21 elevation may be involved in the generation of the beneficial phenotypes seen in knockout animals. Elevated FGF21 levels are seen during insulin resistance (53). However, this elevation is thought to be a compensatory mechanism that is activated in response to hyperglycemia, giving rise to a FGF21 resistance phenotype (54).

$Arv1^{-/-}$ animals showed alterations in bile acid composition in the SI. Of particular interest was the increase seen in TMC. TMC is a potent FXR antagonist, and its accumulation decreases FXR signaling in the intestine (55–57). Intestinal FXR knockout animals have been shown to be resistant to diet-induced obesity, insulin resistance, and NAFLD (58–60). It has also been shown that loss of intestinal FXR activity leads to induced GLP-1 (glucagon-like peptide 1) production, which leads to improved glucose metabolism (61). We saw a larger bile acid pool with a high hydrophobicity index in the SI of $Arv1^{-/-}$ animals. One possible explanation for the presence of this increased pool size may be related to the status of FXR signaling in the SI. FXR activation in the SI induces the transport of intestinal bile acids into the portal vein for recycling back to the liver (62). The accumulation of TMC in $Arv1^{-/-}$ animals would presumably cause FXR inhibition, which would lead to a reduction in bile acid recycling back to the liver and thus a larger bile acid pool. Studies using FXR knockout animals have shown that their total bile acid pool size is increased compared with WT animals (63). It is interesting that *Arv1* ASO treatment in mice activates the FXR pathway in the liver (20). We saw the same in the livers of $Arv1^{-/-}$ animals. This may suggest that $Arv1^{-/-}$ animals have opposing FXR signaling activities, where it exists in an activated state in the liver while being inhibited in the SI.

Our $Arv1^{-/-}$ animals also excreted higher levels of fecal cholesterol and fatty acid but lower levels of TAGs. Our hypothesis is that increased cholesterol excretion may be due to a higher bile acid hydrophobicity index causing less fat solubilization. In the case of the lower TAG excretion, loss of *Arv1* may result in monoacylglycerol acyltransferase (MGAT) and/or diacylglycerol acyltransferase (DGAT) inhibition (64). In this scenario, pancreatic lipase would convert TAGs to monoacylglycerol and FFAs (65), which are substrates for intestinal TAG resynthesis by MGAT and DGAT. Inhibition of MGAT and/or DGAT may explain why we see an increase in fecal excretion of FFA. It is important to point out that monoacylglycerol and diacylglycerol are signaling molecules that regulate multiple metabolic-related events, including fat metabolism in the liver, insulin sensitivity in muscle, and appetite (64).

Drug discovery efforts targeting MGAT inhibition are ongoing for treating metabolic disorders, based on the fact that MGAT2-deficient mice are resistant to diet-induced obesity, NAFLD, hyperlipidemia, and glucose intolerance (66–69).

[5] C. Gallo-Ebert and J. T. Nickels, unpublished data.

DGAT1-deficient mice are also resistant to high-fat diet–induced obesity (70, 71), whereas ASO silencing of DGAT2 results in reduced liver TAGs levels (72). Targeting DGAT1 has met with some difficulty due to severe gastrointestinal side effects (73–75), whereas targeting DGAT2 has been gaining traction (76). Determining whether it is feasible to target ARV1 inhibition for treating MetS awaits further investigation into defining its molecular function.

Lipodystrophy is associated with a deficiency in adipose tissue mass (77). *Arv1*$^{-/-}$ animals are lipodystrophic, as they have severely reduced fat stores, including brown fat. However, these animals show little sign of the hepatic steatosis, insulin resistance, T2D, and hypertriglyceridemia associated with this phenotype (78, 79). They are, however, hyperphagic, but this may be caused by increased energy expenditure. Adipose tissue deficiency leads to the reduced secretion of leptin and adiponectin. Whereas *Arv1*$^{-/-}$ animals do secrete less leptin, they secrete elevated levels of adiponectin. Thus, *Arv1*$^{-/-}$ animals may represent a unique type of lipodystrophy model that is resistant to acquiring multiple metabolic pathologies.

Finally, our *Arv1*$^{-/-}$ animals had reduced levels of HDL whether fed NC or an HFD. Diets high in fat can cause HDL levels to rise in the mouse (80–82), and we observed this in WT animals. In addition to dietary modulation, genetic mouse models have shown that overexpression of human cholesterol ester transfer protein (83) and reductions in apolipoprotein A-I (apoA-I) (84) or apoA-II levels (85, 86) can cause reductions in HDL levels. Interestingly, the C57BL/6J mouse strain used to generate our *Arv1*$^{-/-}$ animals carries the *Ath-1* susceptibility allele that causes reductions in HDL levels when animals are fed an atherogenic diet (87, 88), so differences in dietary content and genetic background can greatly influence HDL metabolism. Interestingly, although HDL levels were reduced in *Arv1*$^{-/-}$ animals, their aortas showed less fatty infiltrate and retained plasticity.[6]

Labor *et al.* (23) have recently examined the metabolic effects brought about by complete loss of *ARV1*. Their *Arv1*$^{-}$/*Arv1*$^{-}$ mice did not gain weight, had improved glucose tolerance, secreted elevated adiponectin levels, had a high metabolic rate, and had less white adipose tissue. A subset of the data presented in this study was obtained using animals fed NC. Here, we examined how *Arv1*$^{-}$/$^{-}$ animals responded metabolically to being fed an HFD. We point out that the KO line described in our paper was generated using a different strain of ES cells and gene targeting strategy as compared with the *Arv1* KO mice described previously (23, 24), indicating that the observed phenotypes are robust and indeed related to the inactivation of the *Arv1* gene. Thus, the current study describes the contribution of *Arv1* to the DIO model phenotypes. Moreover, the model used was congenic to the C57BL/6J strain, the standard mouse strain used for the DIO models commercially available.

Overall, our results strongly suggest that FXR signaling is activated in the livers of *Arv1*$^{-/-}$ animals, which leads to resistance to acquiring diseases associated with MetS and NAFLD under conditions of excess fat consumption (Fig. 18). First, knockout livers had decreased SREBP1-c maturation, possibly leading to the decreases in fatty acid and triglyceride levels observed. Second, liver CYP7α1 and CYP8β1 expressions were attenuated, and these decreases were accompanied by changes in intestinal bile acid composition. In particular, we observed the accumulation of the FXR antagonist, TMC. Interestingly, *Cyp7a1*$^{-/-}$ mice are protected from diet-induced onset of MetS disorders, have an up-regulated alternative bile acid synthetic pathway, and show a moderate increase in TMC (89). TMC accumulation may be the reason for the lack of intestinal FXR signaling observed. Beneficial metabolic effects have been seen when both FXR signaling is inhibited in the intestines but activated in the liver (55, 90).

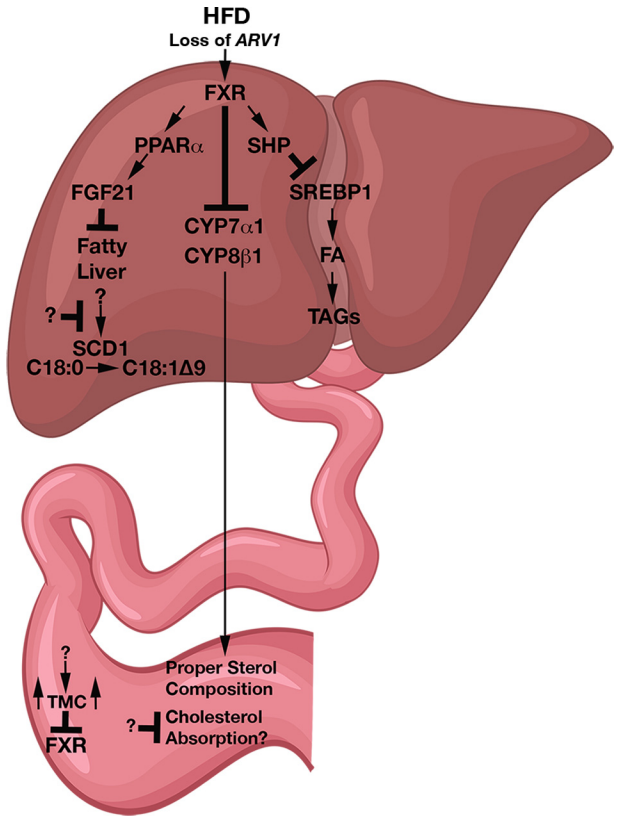

Figure 18. Model showing the effects due to loss of *ARV1*.

Third, PPARα protein levels were increased and there was a concomitant increase in its target, FGF21. Elevated FGF21 levels are thought to attenuate the severity of NAFLD progression (91). Finally, and more speculatively, *Arv1*$^{-/-}$ animals may harbor a malabsorption defect that causes a decrease in dietary fat intake. *Arv1*$^{-/-}$ animals excrete more cholesterol, bile acids, and free fatty acids, and they have an indirect correlation between increased excretion and lower cholesterol and triglycerides blood levels.

In conclusion, we hypothesize that *ARV1* plays a critical role in the development of MetS and NAFLD during conditions of lipid toxicity, possibly by activating liver FXR signaling. Beyond the scope of this work, studies are under way looking at the metabolic phenotypes of *Arv1*$^{-/-}$ *Fxr*$^{-/-}$ animals fed an HFD. The availability of liver and intestinal specific *Fxr* knockouts will precisely define the relationship between ARV1 function and regulation of FXR signaling.

[6] H.-Y. Liu, C. Gallo-Ebert, and J. T. Nickels, unpublished data.

Experimental procedures

Generation of *Arv1*$^{-/-}$ mice

GenOway (Jean Jaures Lyon, France) generated whole-body *Arv1*$^{-/-}$ knockout mice using the Cre-Lox system. Briefly, a homologous recombination targeting construct with a floxed exon 5 and exon 6 was used to produce a stable conditional *ARV1* knockout in C57BL/6J ES cells. Recombinant ES cells were then injected into C57BL/6 albino (B6(Cg)-*Tyr*$^{c-2J}$) recipient blastocysts, followed by implantation into pseudo-pregnant albino C56BL/6 females for the purpose of generating chimera offspring (floxed mice). Upon breeding with C57BL/6 Cre deleter mice, exons 5 and 6 of *Arv1* flanked by loxP sites were excised, resulting in constitutive whole-body *Arv1*$^{-/-}$ knockout mice. Mice were bred to the same C57BL/6J strain to maintain congenicity. Heterozygous parents were crossed to produce homozygous *Arv1*$^{-/-}$ mice. The Invivotek institutional animal care and use committee approved all studies.

Total RNA isolation and quantitative real-time PCR

Total RNA was extracted with TRIzol reagent (Invitrogen). cDNA was synthesized from total RNA using the RT Easy First Strand Kit (Qiagen). Quantitative real-time PCR was carried out using a Stratagene MX3005P (Stratagene). Relative mRNA levels were normalized to levels of glyceraldehyde-3-phosphate dehydrogenase. The data are representative of five independent experiments done in triplicate.

Protein extraction and Western blot analysis

Soon after the mice were euthanized, tissues were dissected and cleaned of adhering fat and soft tissues. They were washed in ice-cold PBS to remove blood from tissues, snap-frozen in liquid nitrogen, and stored at −80 °C until further processing. Tissue lysates were prepared by homogenization in radioimmune precipitation buffer containing phosphatase and protease inhibitors. Tissue debris was removed by centrifugation, and protein concentration was determined using the Bradford assay (Bio-Rad).

For Western blot analysis, we used Ponceau S staining to determine whether the same amount of total protein was loaded and transferred (92, 93). Cell lysates to be analyzed were resuspended in protein sample buffer and incubated at 95 °C for 10 min. All samples were subjected to 10% SDS-PAGE. Resolved proteins were transferred onto a nitrocellulose membrane. The immunoblot membranes were then blocked for 1 h with 10% milk and washed once with TBST (Tris-buffered saline, 0.1% Tween 20) ($n = 8$).

The membranes were incubated with primary antibody overnight, at the appropriate dilution. After five washes with TBST for 10 min each, membranes were incubated with appropriate secondary antibody for 1 h. After five washes with TBST for 10 min, each of the membranes was immersed in chemiluminescent agent and exposed for 2–5 min; β-actin (Abcam) was also used as a loading control at 1:1,000 dilution (Figs. S1–S6).

ARV1 protein levels were determined by chemiluminescence. Anti-ARV1 polyclonal antibodies were from Abgent (catalog no. AP10655a) and used at a 1:500 dilution; anti-SCD1 polyclonal antibodies were from Abcam (catalog no. ab39969) and used at a 1:500 dilution; anti-FXR polyclonal antibodies were from Novus Biologicals (catalog no. NB00-153) and used at a 1:500 dilution; anti-SHP polyclonal antibodies were from Abcam (catalog no. ab96605) and were used at a 1:500 dilution. anti-CYP7α1 polyclonal antibodies were from Abcam (catalog no. ab65596) and were used at a 1:1,000 dilution. anti-CYP8β1 polyclonal antibodies were from Abcam (catalog no. ab191910) and were used at a 1:1,000 dilution. Anti-SREBP1 polyclonal antibodies were from Santa Cruz Biotechnology, Inc. (sc-365513) and were used at a 1:250 dilution. We consistently observed a lot-to-lot variability in the specificity of the Abgent anti-ARV1 antibodies. To circumvent this problem, several lots were tested, and 1 mg of the lot with the highest specificity was purchased and used. The immunoblots shown are representative of three independent Western blot analyses ($n = 8$).

Survival studies

The age of death was recorded for all males used in the HFD and regular diet branches. Data were graphed using a survival curve and analyzed using the Mantel–Cox test (GraphPad Prism version 5).

Rotarod studies

Individually housed male WT and *Arv1*$^{-/-}$ mice aged 9–14 weeks were used for this experiment. Mice were acclimated to the testing room for at least 30 min. The assay was carried out using four EzRod test chambers. For the accelerating rotarod paradigm, mice were given 10 trials with the maximum duration of 3 min and a 30-s intertrial interval. Each mouse was placed on the EZRod machine, and the latency to fall was recorded for all trials. If the mouse fell or 3 min elapsed, the mouse was left in the bottom of the EzRod test chamber for 30 s before starting the next trial.

The latency to fall was compared between the three groups by analysis of variance (ANOVA) with repeated measures using Bonferroni corrected post hoc analysis for pairwise comparisons (GraphPad Prism version 5).

Open field test

Individually housed male WT, and *Arv1*$^{-/-}$ animals aged 10–14 weeks were used for this experiment. The assay was performed in a custom-made open field apparatus. Each chamber is a 50 × 50-cm square. The experiment is recorded and tracked by a tracking system obtained from Viewpoint.

The time and the path length in the center of the open field were determined. The center of the open field was defined as a 13.5 × 13.5-cm square in the geometric center of the arena. The percent of path in the center was calculated as follows: Path length in the center × 100%/total path length.

For each mouse, the total path length and path length for 30 min at 5-min intervals were determined as measures of locomotor activity. Each chamber was cleaned between individual tests.

Path lengths for 30 min at 5-min intervals were analyzed by a two-way ANOVA with time as a within-subjects (repeated measures) factor and genotype as a between-groups factor using GraphPad Prism version 5.0. All other parameters were compared using a one-way ANOVA (GraphPad Prism).

Fertility assay

Male fertility—Sexually mature males (~3 months old) were paired with two ICR females (6 weeks old) on day 1.

Female fertility—Sexually mature females (6–7 weeks old) were paired with an ICR male (8 weeks old) on day 1. The presence of a vaginal plug was checked every day for 6 days, and then the male was removed. Females were checked daily, and size and birth dates of litters were recorded. Litter size was analyzed by a one-way ANOVA. The Mann–Whitney test was used to analyze the number of days, and χ^2 was used to analyze the plug/no plug and litter/no litter data (GraphPad Prism version 5).

Longitudinal body weights and diet challenge

Individually housed male *Arv1*$^{-/-}$ and WT mice were maintained on a 12-h light/dark cycle with food and water fed *ad libitum* unless otherwise noted. Mice were initially maintained on a regular chow diet (Purina rodent diet catalog no. 5053, W. F. Fisher and Son, Bound Brook, NJ), and baseline body weights were established when the mice were 8 weeks old. At age 12 weeks, mice were either left on normal chow or switched to an HFD (60% fat, D12492, Research Diets, New Brunswick, NJ), and body weights were collected over an 11-week period (Fig. 6). The mice were divided into three branches with eight males in each. Branch A was fed NC for the entire study. Branch B animals were given normal chow for the first 4 weeks and then switched to an HFD for 11 weeks. Branch C mice were sacrificed at the beginning of the study. In some studies, a Western diet (RD12079B Research Diets, New Brunswick, NJ) was used as the high-fat diet. Body weights were analyzed by a two-way ANOVA with genotype as a between-group factor and the time course as a within-subject factor (repeated measures).

Adiponectin and leptin determination

Blood was collected from the retro-orbital sinus under isoflurane anesthesia from mice fasted overnight. The blood was allowed to coagulate for 30 min at room temperature and centrifuged at 1000 × *g* for 15 min at 4 °C to collect serum. The serum was immediately frozen and stored at −80 °C. Adiponectin concentrations were determined from serum samples by electrochemiluminscence (MA2400 mouse adiponectin kit K152BXC, Meso Scale Discovery). Serum leptin concentrations were determined by electrochemiluminescence according to the manufacturer's recommendations (MS2400 mouse leptin kit, K152BYC-2 Meso Scale Discovery). Data were analyzed by an unpaired *t* test.

Ghrelin determination

Blood samples were collected in tubes containing EDTA (0.5 mg/ml final, 1:40 dilution) and polyhexamethylene biguanide (0.4 mM final, 1:100 dilution) to prevent degradation of acylated ghrelin by proteases. Samples were centrifuged at 4,000 rpm for 10 min at 4 °C, and supernatants were transferred to separate tubes. 1 N HCl was added at a 1:10 dilution. Samples were frozen at −80 °C, and acyl and deacyl ghrelin concentrations in plasma were evaluated by a specific enzyme immunoassay (SPIbio Bertin Pharma): A05118 for the deacylated form and A05117 for the acylated form.

Adipose distribution

Adipose tissue dissections were performed on 18–21-week-old males following 11 weeks on an HFD. Adipose tissue was from the inguinal fat pad (subcutaneous), and the visceral fat was from the epididymal, renal (retroperitoneal), and mesenteric fat depots. The data were analyzed by an unpaired *t* test for each adipose depot individually.

Metabolic studies

Metabolic studies were performed using the Comprehensive Cage Monitoring System (Columbus Instruments, Columbus, OH). This system allows for the long-term automated, noninvasive simultaneous collection of nine measurements. The experimental window lasted 48 h, beginning and ending at the start of the dark phase of the light cycle. During that time the following end points were measured: heat (kcal/kg/h (calculated by the Oxymax Software using O_2 consumption, CO_2 production, and body weight)); VO_2 (oxygen consumption in ml/kg/h (calculated by the Oxymax software using O_2 differential and body weight)); VCO_2 (carbon dioxide production in ml/kg/h (calculated by the Oxymax software using CO_2 differential and body weight)); and respiratory exchange ratio (VCO_2/VO_2) (calculated by the Oxymax software).

Oxygen and carbon dioxide concentrations were sequentially measured. The time required for a single round of gas measurements in all of the chambers was defined as an interval. The interval lengths may have varied slightly, depending on the environmental parameters of the room (temperature and humidity) and the physiological parameters of the experimental mice. On average, each interval was 48 min.

For statistical analysis, all data were averaged into individual days. Data were analyzed by a two-way ANOVA. The Bonferroni adjusted post hoc procedure was used for pairwise comparisons. The body weights of the animals were measured before placing the mice in the CCMS chambers and when they were removed after 48 h; the change in body weight was used as a covariate in the ANOVA analysis of VO_2, VCO_2, and energy expenditure, as these measures use body weight as a constant in their calculation.

Serum cholesterol levels

Serum cholesterol levels were measured in WT and *Arv1*$^{-/-}$ male mice after an overnight fast (16 h) at the time points shown (Fig. 6). Blood was collected from the retro-orbital sinus, and cholesterol concentrations were determined enzymatically from serum (Thermo DMA, Arlington, TX). An unpaired *t* test was used to analyze differences between the genotypes.

Triglyceride assay

Triglyceride levels were measured after an overnight fast (16 h) (Fig. 6). Whole blood was collected via the retro-orbital sinus, and triglycerides were assessed using a hand-held meter (CardioChek, PTS Inc., Indianapolis, IN) with test strips specific for triglyceride measurements. An unpaired *t* test was used to analyze differences between the genotypes.

Body composition by DEXA

DEXA was performed at the indicated times (Fig. 6). The body composition was assessed using the PIXImus2 X-ray unit (GE Lunar Corp., Madison, WI), excluding the head region. An unpaired *t* test was used to analyze any differences between the genotypes for each measurement.

Oral glucose tolerance test and insulin measurements

The OGTT was performed after an overnight fast (~16 h) (Fig. 6). Blood glucose levels were measured using a One-touch Ultra 2 (Lifescan, Johnson & Johnson) glucometer at baseline, just before the mice received 2 g/kg of body weight of 100 mg/ml glucose delivered by oral gavage. Blood glucose was subsequently measured 15, 30, 60, and 120 min after the administration of glucose. Parallel samples for measuring plasma insulin levels were also collected and assayed by electrochemiluminscence (MA2400 Mouse/Rat insulin kit K152BZC, Meso Scale Discovery).

Glucose and insulin results were analyzed by a two-way ANOVA with genotype as a between-group factor and the time course as a within-subject factor (repeated measures). The pregavage blood glucose and insulin levels were used as the baseline values for calculating the AUC for each subject. Baseline blood glucose and plasma insulin levels and AUC data were also analyzed by an unpaired *t* test comparing results from the diets separately.

Insulin tolerance test

Before testing, the mice were fasted for 4 h. Blood was obtained from a tail cut (by removing the distal 2 mm of the tail) and was assessed for baseline glucose levels using a One-touch Ultra 2 (Lifescan, Johnson & Johnson) glucometer. The mice then received the indicated concentration of normal insulin (Novolin R) by intraperitoneal injection. At 15, 30, 60, 90, and 120 min after the administration of insulin, dried blood and tissue were quickly removed from the tail wound to measure the blood glucose concentration.

Lipid extraction

100 mg of liver, small intestine tissues, or feces was homogenized using a mortar and pestle. The resulting homogenate was extracted with 18 volumes of a mixture of hexane/2-propanol (3:2) for 1 min in 15-ml conical tubes. Samples were vortexed for 20 min at low speed (2,000 rpm) and subsequently centrifuged at 5,000 × *g* for 4 min at 4 °C. The supernatant was transferred to a glass conical tube and subsequently washed with one-fifth volume of 0.9% NaCl. The sample was centrifuged at 5,000 × *g* for 4 min at 4 °C, and the aqueous phase was removed. The lower phase was dried down under a stream of nitrogen and resuspended in isopropyl alcohol until use (94).

Apolipoprotein analysis

HDL, LDL, and very low-density apolipoprotein (VLDL) levels were measured using the LipoPrint LDL system (LipoPrint LDL Subfraction kit, catalog no. 48-7002; Quantimetrix, Redondo Beach, CA) according to the manufacturer's instructions. The results from the LipoPrint system are directly quantified as a relative percentage for each sized particle, so absolute amounts of each particle were calculated using the relative percentage from the LipoPrint system and the quantity of total cholesterol measured in the previous total cholesterol assay (percentage of total cholesterol × total cholesterol).

Hepatic triglyceride export assay

Mice fed NC were fasted for 4 h. They were then dosed with 500 mg/kg Pluronic F127 (Polaxamer 404) by intraperitoneal injection. 5 ml/kg olive oil was given to each animal. Blood was then obtained from the tail vein at the indicated times. TAG levels were determined using the L-type triglyceride M microtiter Procedure (WAKO).

Histology

Tissues were fixed in 10% neutral-buffered formalin, processed for 12 h using Thermo Scientific Excelsior ES, embedded in paraffin blocks, and cut on 4 μm using a Sakura SRM200 microtome. Leica manufacturing protocols were used for H&E staining. All stains were performed on a Leica ST5020 automated stainer. H&E-processed tissues mounted on glass slides were examined using a Nikon Eclipse 50i clinical microscope. Tissues were examined under ×4, ×10, and ×40 magnification. Pictures were taken with an INFINITY 1-2CB microscope camera. The chronic hepatitis assessment scheme used for this study was the Scheuer Classification for Grading and Staging of Chronic Hepatitis (95).

Serum clinical chemistries

Serum was collected by a cardiac bleed from 18–21–week-old *Arv1*$^{-/-}$ ($n = 4$) and WT ($n = 8$) mice following 11 weeks on an HFD and analyzed on an ACE Alera (Alfa Wasserman) for multiple analytes according to the manufacturer's instructions.

Lipid level assays

20 μl of sample, calibrator, and control were added to 150 μl of reconstituted reagent CC3 in a microplate. The reaction was mixed well by repeated pipetting. The plate was incubated at 37 °C for 5 min. 30 μl of reagent CC2 was mixed in the reaction. The increase in absorbance after 5 min at 37 °C was measured using a plate reader at 540 nm. BA concentration = ((sample A_{540} − blank A_{540})/(calibrator A_{540} − blank A_{540})) × calibrator concentration.

Samples were brought up in assay buffer. 2 μl of acyl-CoA synthesis reagent was added to each sample and mixed. Samples were incubated at 37 °C for 30 min. A reaction mix containing assay buffer (44 μl), fatty acid probe (2 μl), enzyme mix (2 μl), and enhancer (2 μl) was added. Samples were mixed and incubated for 30 min at 37 °C in the dark. A_{570} was measured in a microplate reader. FFA concentration = FA/Sv (mM), where FA is the fatty acid amount in the well obtained from the standard curve, and Sv is the sample volume added to the sample well. Samples were brought up in assay buffer.

Liver fatty-acid analysis

Fatty acids were extracted from frozen, homogenized tissue and were saponified by a modified Bligh–Dyer method (96). Fatty acids were converted to methyl esters by treatment with

boron trifluoride and analyzed by GC on a Hewlett-Packard model 6890 gas chromatograph using a 30-m HP-5 column. Instrument conditions were as described previously (97). Identification of fatty acid species was by comparing the retention times with those of authentic standards (Nu-Chek Prep) or by GC/MS analysis.

Small intestine bile acid analysis

Bile acid analysis was performed as described (41).

Author contributions—C. G.-E., H-Y. L., M. D. H., B. K. J., O. B., V. M., and J. T. N. conceptualization; C. G.-E., J. F., H-Y. L., R. D., K. M., M. D. H., B. K. J., and V. M. investigation; O. B. and J. T. N. data curation; J. T. N. formal analysis.

Acknowledgments—We acknowledge the histology work performed by Dr. Jing Jing Yang and Mariya Nestor at the Institute of Biomarker Research. We acknowledge the Cohen Laboratory for analyzing bile acid composition. We thank Pedro Martins and Elka Devash for the graphic design in Fig. 18. We appreciate the discussions with our colleagues at the Institute of Metabolic Disorders, Invivotek, Oncoveda, Femeris, and Genesis Biotechnology Group. We appreciate the intellectual conversations with Drs. Eli Mordechai and Martin Adelson. We acknowledge the many members of the Invivotek team for their expertise.

References

1. Dietrich, P., and Hellerbrand, C. (2014) Non-alcoholic fatty liver disease, obesity and the metabolic syndrome. *Best Pract. Res. Clin. Gastroenterol.* **28,** 637–653 CrossRef Medline
2. Fulop, T., Tessier, D., and Carpentier, A. (2006) The metabolic syndrome. *Pathol. Biol.* **54,** 375–386 CrossRef Medline
3. Kaur, J. (2014) A comprehensive review on metabolic syndrome. *Cardiol. Res. Pract.* **2014,** 943162 Medline
4. Byrne, C. D., and Targher, G. (2015) NAFLD: a multisystem disease. *J. Hepatol.* **62,** S47–S64 CrossRef Medline
5. Alberti, K. G., Zimmet, P., and Shaw, J. (2006) Metabolic syndrome: a new world-wide definition: a consensus statement from the International Diabetes Federation. *Diabet. Med.* **23,** 469–480 CrossRef Medline
6. Ruderman, N., Chisholm, D., Pi-Sunyer, X., and Schneider, S. (1998) The metabolically obese, normal-weight individual revisited. *Diabetes* **47,** 699–713 CrossRef Medline
7. Than, N. N., and Newsome, P. N. (2015) A concise review of non-alcoholic fatty liver disease. *Atherosclerosis* **239,** 192–202 CrossRef Medline
8. Targher, G., Marchesini, G., and Byrne, C. D. (2016) Risk of type 2 diabetes in patients with non-alcoholic fatty liver disease: causal association or epiphenomenon? *Diabetes Metab.* **42,** 142–156 CrossRef Medline
9. Loomba, R., and Sanyal, A. J. (2013) The global NAFLD epidemic. *Nat. Rev. Gastroenterol. Hepatol.* **10,** 686–690 CrossRef Medline
10. Samuel, V. T., and Shulman, G. I. (2018) Nonalcoholic fatty liver disease as a nexus of metabolic and hepatic diseases. *Cell Metab.* **27,** 22–41 CrossRef Medline
11. Gluchowski, N. L., Becuwe, M., Walther, T. C., and Farese, R. V., Jr. (2017) Lipid droplets and liver disease: from basic biology to clinical implications. *Nat. Rev. Gastroenterol. Hepatol.* **14,** 343–355 CrossRef Medline
12. Saltiel, A. R., and Kahn, C. R. (2001) Insulin signalling and the regulation of glucose and lipid metabolism. *Nature* **414,** 799–806 CrossRef Medline
13. Tinkelenberg, A. H., Liu, Y., Alcantara, F., Khan, S., Guo, Z., Bard, M., and Sturley, S. L. (2000) Mutations in yeast ARV1 alter intracellular sterol distribution and are complemented by human ARV1. *J. Biol. Chem.* **275,** 40667–44070 CrossRef Medline
14. Swain, E., Stukey, J., McDonough, V., Germann, M., Liu, Y., Sturley, S. L., and Nickels, J. T., Jr. (2002) Yeast cells lacking the ARV1 gene harbor defects in sphingolipid metabolism. Complementation by human ARV1. *J. Biol. Chem.* **277,** 36152–36160 CrossRef Medline
15. Kajiwara, K., Watanabe, R., Pichler, H., Ihara, K., Murakami, S., Riezman, H., and Funato, K. (2008) Yeast ARV1 is required for efficient delivery of an early GPI intermediate to the first mannosyltransferase during GPI assembly and controls lipid flow from the endoplasmic reticulum. *Mol. Biol. Cell* **19,** 2069–2082 CrossRef Medline
16. Villasmil, M. L., Ansbach, A., and Nickels, J. T., Jr. (2011) The putative lipid transporter, Arv1, is required for activating pheromone-induced MAP kinase signaling in *Saccharomyces cerevisiae*. *Genetics* **187,** 455–465 CrossRef Medline
17. Georgiev, A. G., Johansen, J., Ramanathan, V. D., Sere, Y. Y., Beh, C. T., and Menon, A. K. (2013) Arv1 regulates PM and ER membrane structure and homeostasis but is dispensable for intracellular sterol transport. *Traffic* **14,** 912–921 CrossRef Medline
18. Schechtman, C. F., Henneberry, A. L., Seiman, T. A., Tinkelenberg, A. H., Wilcox, L. J., Lee, E., Fazlollahi, M., Bussemaker, H. J., Tabas, I., and Sturley, S. L. (2011) Loss of subcellular lipid transport due to ARV1 deficiency disrupts organelle homeostasis and activates the unfolded protein response. *J. Biol. Chem.* **286,** 11951–11959 CrossRef Medline
19. Ruggles, K. V., Garbarino, J., Liu, Y., Moon, J., Schneider, K., Henneberry, A., Billheimer, J., Millar, J. S., Marchadier, D., Valasek, M. A., Joblin-Mills, A., Gulati, S., Munkacsi, A. B., Repa, J. J., Rader, D., and Sturley, S. L. (2014) A functional, genome-wide evaluation of liposensitive yeast identifies the "ARE2 required for viability" (ARV1) gene product as a major component of eukaryotic fatty acid resistance. *J. Biol. Chem.* **289,** 4417–4431 CrossRef Medline
20. Tong, F., Billheimer, J., Shechtman, C. F., Liu, Y., Crooke, R., Graham, M., Cohen, D. E., Sturley, S. L., and Rader, D. J. (2010) Decreased expression of ARV1 results in cholesterol retention in the endoplasmic reticulum and abnormal bile acid metabolism. *J. Biol. Chem.* **285,** 33632–33641 CrossRef Medline
21. Hulce, J. J., Cognetta, A. B., Niphakis, M. J., Tully, S. E., and Cravatt, B. F. (2013) Proteome-wide mapping of cholesterol-interacting proteins in mammalian cells. *Nat. Methods* **10,** 259–264 CrossRef Medline
22. Niphakis, M. J., Lum, K. M., Cognetta, A. B., 3rd, Correia, B. E., Ichu, T. A., Olucha, J., Brown, S. J., Kundu, S., Piscitelli, F., Rosen, H., and Cravatt, B. F. (2015) A global map of lipid-binding proteins and their ligandability in cells. *Cell* **161,** 1668–1680 CrossRef Medline
23. Lagor, W. R., Tong, F., Jarrett, K. E., Lin, W., Conlon, D. M., Smith, M., Wang, M. Y., Yenilmez, B. O., McCoy, M. G., Fields, D. W., O'Neill, S. M., Gupta, R., Kumaravel, A., Redon, V., Ahima, R. S., *et al.* (2015) Deletion of murine Arv1 results in a lean phenotype with increased energy expenditure. *Nutr. Diabetes* **5,** e181 CrossRef Medline
24. Palmer, E. E., Jarrett, K. E., Sachdev, R. K., Al Zahrani, F., Hashem, M. O., Ibrahim, N., Sampaio, H., Kandula, T., Macintosh, R., Gupta, R., Conlon, D. M., Billheimer, J. T., Rader, D. J., Funato, K., Walkey, C. J., *et al.* (2016) Neuronal deficiency of ARV1 causes an autosomal recessive epileptic encephalopathy. *Hum. Mol. Genet.* **25,** 3042–3054 Medline
25. Deacon, R. M. (2013) Measuring motor coordination in mice. *J. Vis. Exp.* e2609 CrossRef Medline
26. Wall, P. M., and Messier, C. (2000) Concurrent modulation of anxiety and memory. *Behav. Brain Res.* **109,** 229–241 CrossRef Medline
27. Warita, K., Sugawara, T., Yue, Z. P., Tsukahara, S., Mutoh, K., Hasegawa, Y., Kitagawa, H., Mori, C., and Hoshi, N. (2006) Progression of the dose-related effects of estrogenic endocrine disruptors, an important factor in declining fertility, differs between the hypothalamo-pituitary axis and reproductive organs of male mice. *J. Vet. Med. Sci.* **68,** 1257–1267 CrossRef Medline
28. Wang, H. Y., Li, Y. H., Sun, L., Gao, X., You, L., Wang, Y., Ma, J. L., and Chen, Z. J. (2013) Allotransplantation of cryopreserved prepubertal mouse ovaries restored puberty and fertility without affecting methylation profile of Snrpn-DMR. *Fertil. Steril.* **99,** 241–247 CrossRef Medline
29. Khan, A., Bellefontaine, N., and deCatanzaro, D. (2008) Onset of sexual maturation in female mice as measured in behavior and fertility: interactions of exposure to males, phytoestrogen content of diet, and ano-genital distance. *Physiol. Behav.* **93,** 588–594 CrossRef Medline

30. Klok, M. D., Jakobsdottir, S., and Drent, M. L. (2007) The role of leptin and ghrelin in the regulation of food intake and body weight in humans: a review. *Obes. Rev.* **8,** 21–34 CrossRef Medline
31. Flak, J. N., and Myers, M. G., Jr. (2016) Minireview: CNS mechanisms of leptin action. *Mol. Endocrinol.* **30,** 3–12 CrossRef Medline
32. Balsan, G. A., Vieira, J. L., Oliveira, A. M., and Portal, V. L. (2015) Relationship between adiponectin, obesity and insulin resistance. *Rev. Assoc. Med. Bras.* **61,** 72–80 CrossRef Medline
33. Fasshauer, M., and Blüher, M. (2015) Adipokines in health and disease. *Trends Pharmacol. Sci.* **36,** 461–470 CrossRef Medline
34. Aguilar-Salinas, C. A., García, E. G., Robles, L., Riaño, D., Ruiz-Gomez, D. G., García-Ulloa, A. C., Melgarejo, M. A., Zamora, M., Guillen-Pineda, L. E., Mehta, R., Canizales-Quinteros, S., Tusie Luna, M. T., and Gómez-Pérez, F. J. (2008) High adiponectin concentrations are associated with the metabolically healthy obese phenotype. *J. Clin. Endocrinol. Metab.* **93,** 4075–4079 CrossRef Medline
35. Fazio, S., and Linton, M. F. (2001) Mouse models of hyperlipidemia and atherosclerosis. *Front. Biosci.* **6,** D515–D525 CrossRef Medline
36. Fontaine, D. A., and Davis, D. B. (2016) Attention to background strain is essential for metabolic research: C57BL/6 and the International Knockout Mouse Consortium. *Diabetes* **65,** 25–33 CrossRef Medline
37. Ioannou, G. N. (2016) The role of cholesterol in the pathogenesis of NASH. *Trends Endocrinol. Metab.* **27,** 84–95 CrossRef Medline
38. Koo, S. H. (2013) Nonalcoholic fatty liver disease: molecular mechanisms for the hepatic steatosis. *Clin. Mol. Hepatol.* **19,** 210–215 CrossRef Medline
39. Liu, W., Baker, R. D., Bhatia, T., Zhu, L., and Baker, S. S. (2016) Pathogenesis of nonalcoholic steatohepatitis. *Cell. Mol. Life Sci.* **73,** 1969–1987 CrossRef Medline
40. Scheuer, P. J. (1991) Classification of chronic viral hepatitis: a need for reassessment. *J. Hepatol.* **13,** 372–374 CrossRef Medline
41. Rossi, S. S., Converse, J. L., and Hofmann, A. F. (1987) High pressure liquid chromatographic analysis of conjugated bile acids in human bile: simultaneous resolution of sulfated and unsulfated lithocholyl amidates and the common conjugated bile acids. *J. Lipid Res.* **28,** 589–595 Medline
42. Gallo-Ebert, C., McCourt, P. C., Donigan, M., Villasmil, M. L., Chen, W., Pandya, D., Franco, J., Romano, D., Chadwick, S. G., Gygax, S. E., and Nickels, J. T., Jr. (2012) Arv1 lipid transporter function is conserved between pathogenic and nonpathogenic fungi. *Fungal Genet. Biol.* **49,** 101–113 CrossRef Medline
43. Villasmil, M. L., and Nickels, J. T., Jr. (2011) Determination of the membrane topology of Arv1 and the requirement of the ER luminal region for Arv1 function in *Saccharomyces cerevisiae*. *FEMS Yeast Res.* **11,** 524–527 CrossRef Medline
44. Berry, R., Schaid, D. J., Smith, J. R., French, A. J., Schroeder, J. J., McDonnell, S. K., Peterson, B. J., Wang, Z. Y., Carpten, J. D., Roberts, S. G., Tester, D. J., Blute, M. L., Trent, J. M., and Thibodeau, S. N. (2000) Linkage analyses at the chromosome 1 loci 1q24-25 (HPC1), 1q42.2-43 (PCAP), and 1p36 (CAPB) in families with hereditary prostate cancer. *Am. J. Hum. Genet.* **66,** 539–546 CrossRef Medline
45. Feitosa, M. F., Borecki, I. B., Rankinen, T., Rice, T., Després, J. P., Chagnon, Y. C., Gagnon, J., Leon, A. S., Skinner, J. S., Bouchard, C., Province, M. A., and Rao, D. C. (2005) Evidence of QTLs on chromosomes 1q42 and 8q24 for LDL-cholesterol and apoB levels in the HERITAGE family study. *J. Lipid Res.* **46,** 281–286 CrossRef Medline
46. Alazami, A. M., Patel, N., Shamseldin, H. E., Anazi, S., Al-Dosari, M. S., Alzahrani, F., Hijazi, H., Alshammari, M., Aldahmesh, M. A., Salih, M. A., Faqeih, E., Alhashem, A., Bashiri, F. A., Al-Owain, M., Kentab, A. Y., *et al.* (2015) Accelerating novel candidate gene discovery in neurogenetic disorders via whole-exome sequencing of prescreened multiplex consanguineous families. *Cell Rep.* **10,** 148–161 CrossRef Medline
47. Crujeiras, A. B., Carreira, M. C., Cabia, B., Andrade, S., Amil, M., and Casanueva, F. F. (2015) Leptin resistance in obesity: an epigenetic landscape. *Life Sci.* **140,** 57–63 CrossRef Medline
48. Padmalayam, I., and Suto, M. (2013) Role of adiponectin in the metabolic syndrome: current perspectives on its modulation as a treatment strategy. *Curr. Pharm. Des.* **19,** 5755–5763 CrossRef Medline
49. López-Jaramillo, P., Gómez-Arbeláez, D., López-López, J., López-López, C., Martínez-Ortega, J., Gómez-Rodríguez, A., and Triana-Cubillos, S. (2014) The role of leptin/adiponectin ratio in metabolic syndrome and diabetes. *Horm. Mol. Biol. Clin. Investig.* **18,** 37–45 Medline
50. Yoon, M. J., Lee, G. Y., Chung, J. J., Ahn, Y. H., Hong, S. H., and Kim, J. B. (2006) Adiponectin increases fatty acid oxidation in skeletal muscle cells by sequential activation of AMP-activated protein kinase, p38 mitogen-activated protein kinase, and peroxisome proliferator-activated receptor α. *Diabetes* **55,** 2562–2570 CrossRef Medline
51. Mai, K., Andres, J., Biedasek, K., Weicht, J., Bobbert, T., Sabath, M., Meinus, S., Reinecke, F., Möhlig, M., Weickert, M. O., Clemenz, M., Pfeiffer, A. F., Kintscher, U., Spuler, S., and Spranger, J. (2009) Free fatty acids link metabolism and regulation of the insulin-sensitizing fibroblast growth factor-21. *Diabetes* **58,** 1532–1538 CrossRef Medline
52. Liu, J., Xu, Y., Hu, Y., and Wang, G. (2015) The role of fibroblast growth factor 21 in the pathogenesis of non-alcoholic fatty liver disease and implications for therapy. *Metabolism* **64,** 380–390 CrossRef Medline
53. Chavez, A. O., Molina-Carrion, M., Abdul-Ghani, M. A., Folli, F., Defronzo, R. A., and Tripathy, D. (2009) Circulating fibroblast growth factor-21 is elevated in impaired glucose tolerance and type 2 diabetes and correlates with muscle and hepatic insulin resistance. *Diabetes Care* **32,** 1542–1546 CrossRef Medline
54. Emanuelli, B., Vienberg, S. G., Smyth, G., Cheng, C., Stanford, K. I., Arumugam, M., Michael, M. D., Adams, A. C., Kharitonenkov, A., and Kahn, C. R. (2014) Interplay between FGF21 and insulin action in the liver regulates metabolism. *J. Clin. Invest.* **124,** 515–527 CrossRef Medline
55. Xie, C., Jiang, C., Shi, J., Gao, X., Sun, D., Sun, L., Wang, T., Takahashi, S., Anitha, M., Krausz, K. W., Patterson, A. D., and Gonzalez, F. J. (2017) An intestinal farnesoid X receptor-ceramide signaling axis modulates hepatic gluconeogenesis in mice. *Diabetes* **66,** 613–626 CrossRef Medline
56. Qi, Y., Jiang, C., Cheng, J., Krausz, K. W., Li, T., Ferrell, J. M., Gonzalez, F. J., and Chiang, J. Y. (2015) Bile acid signaling in lipid metabolism: metabolomic and lipidomic analysis of lipid and bile acid markers linked to anti-obesity and anti-diabetes in mice. *Biochim. Biophys. Acta* **1851,** 19–29 CrossRef Medline
57. Sayin, S. I., Wahlström, A., Felin, J., Jäntti, S., Marschall, H. U., Bamberg, K., Angelin, B., Hyötyläinen, T., Orešič, M., and Bäckhed, F. (2013) Gut microbiota regulates bile acid metabolism by reducing the levels of tauro-β-muricholic acid, a naturally occurring FXR antagonist. *Cell Metab.* **17,** 225–235 CrossRef Medline
58. de Boer, J. F., Schonewille, M., Boesjes, M., Wolters, H., Bloks, V. W., Bos, T., van Dijk, T. H., Jurdzinski, A., Boverhof, R., Wolters, J. C., Kuivenhoven, J. A., van Deursen, J. M., Oude Elferink, R. P. J., Moschetta, A., Kremoser, C., *et al.* (2017) Intestinal farnesoid X receptor controls transintestinal cholesterol excretion in mice. *Gastroenterology* **152,** 1126–1138.e6 CrossRef Medline
59. Parséus, A., Sommer, N., Sommer, F., Caesar, R., Molinaro, A., Ståhlman, M., Greiner, T. U., Perkins, R., and Bäckhed, F. (2017) Microbiota-induced obesity requires farnesoid X receptor. *Gut* **66,** 429–437 CrossRef Medline
60. Sun, R., Yang, N., Kong, B., Cao, B., Feng, D., Yu, X., Ge, C., Huang, J., Shen, J., Wang, P., Feng, S., Fei, F., Guo, J., He, J., Aa, N., *et al.* (2017) Orally administered berberine modulates hepatic lipid metabolism by altering microbial bile acid metabolism and the intestinal FXR signaling pathway. *Mol. Pharmacol.* **91,** 110–122 CrossRef Medline
61. Trabelsi, M. S., Daoudi, M., Prawitt, J., Ducastel, S., Touche, V., Sayin, S. I., Perino, A., Brighton, C. A., Sebti, Y., Kluza, J., Briand, O., Dehondt, H., Vallez, E., Dorchies, E., Baud, G., *et al.* (2015) Farnesoid X receptor inhibits glucagon-like peptide-1 production by enteroendocrine L cells. *Nat. Commun.* **6,** 7629 CrossRef Medline
62. Dawson, P. A. (2011) Role of the intestinal bile acid transporters in bile acid and drug disposition. *Handb. Exp. Pharmacol.* 169–203 CrossRef Medline
63. Kok, T., Hulzebos, C. V., Wolters, H., Havinga, R., Agellon, L. B., Stellaard, F., Shan, B., Schwarz, M., and Kuipers, F. (2003) Enterohepatic circulation of bile salts in farnesoid X receptor-deficient mice: efficient intestinal bile salt absorption in the absence of ileal bile acid-binding protein. *J. Biol. Chem.* **278,** 41930–41937 CrossRef Medline

64. Shi, Y., and Cheng, D. (2009) Beyond triglyceride synthesis: the dynamic functional roles of MGAT and DGAT enzymes in energy metabolism. *Am. J. Physiol. Endocrinol. Metab.* **297,** E10–E18 CrossRef Medline
65. Brownlee, I. A., Forster, D. J., Wilcox, M. D., Dettmar, P. W., Seal, C. J., and Pearson, J. P. (2010) Physiological parameters governing the action of pancreatic lipase. *Nutr. Res. Rev.* **23,** 146–154 CrossRef Medline
66. Ohshiro, T., and Tomoda, H. (2015) Acyltransferase inhibitors: a patent review (2010-present). *Expert Opin. Ther. Pat.* **25,** 145–158 CrossRef Medline
67. Nelson, D. W., Gao, Y., Spencer, N. M., Banh, T., and Yen, C. L. (2011) Deficiency of MGAT2 increases energy expenditure without high-fat feeding and protects genetically obese mice from excessive weight gain. *J. Lipid Res.* **52,** 1723–1732 CrossRef Medline
68. Yen, C. L., Cheong, M. L., Grueter, C., Zhou, P., Moriwaki, J., Wong, J. S., Hubbard, B., Marmor, S., and Farese, R. V., Jr. (2009) Deficiency of the intestinal enzyme acyl CoA:monoacylglycerol acyltransferase-2 protects mice from metabolic disorders induced by high-fat feeding. *Nat. Med.* **15,** 442–446 CrossRef Medline
69. Banh, T., Nelson, D. W., Gao, Y., Huang, T. N., Yen, M. I., and Yen, C. L. (2015) Adult-onset deficiency of acyl CoA:monoacylglycerol acyltransferase 2 protects mice from diet-induced obesity and glucose intolerance. *J. Lipid Res.* **56,** 379–389 CrossRef Medline
70. Smith, S. J., Cases, S., Jensen, D. R., Chen, H. C., Sande, E., Tow, B., Sanan, D. A., Raber, J., Eckel, R. H., and Farese, R. V., Jr. (2000) Obesity resistance and multiple mechanisms of triglyceride synthesis in mice lacking Dgat. *Nat. Genet.* **25,** 87–90 CrossRef Medline
71. Chen, H. C., Smith, S. J., Ladha, Z., Jensen, D. R., Ferreira, L. D., Pulawa, L. K., McGuire, J. G., Pitas, R. E., Eckel, R. H., and Farese, R. V., Jr. (2002) Increased insulin and leptin sensitivity in mice lacking acyl CoA:diacylglycerol acyltransferase 1. *J. Clin. Invest.* **109,** 1049–1055 CrossRef Medline
72. Liu, Y., Millar, J. S., Cromley, D. A., Graham, M., Crooke, R., Billheimer, J. T., and Rader, D. J. (2008) Knockdown of acyl-CoA:diacylglycerol acyltransferase 2 with antisense oligonucleotide reduces VLDL TG and ApoB secretion in mice. *Biochim. Biophys. Acta* **1781,** 97–104 CrossRef Medline
73. Gluchowski, N. L., Chitraju, C., Picoraro, J. A., Mejhert, N., Pinto, S., Xin, W., Kamin, D. S., Winter, H. S., Chung, W. K., Walther, T. C., and Farese, R. V., Jr. (2017) Identification and characterization of a novel DGAT1 missense mutation associated with congenital diarrhea. *J. Lipid Res.* **58,** 1230–1237 CrossRef Medline
74. Denison, H., Nilsson, C., Löfgren, L., Himmelmann, A., Mårtensson, G., Knutsson, M., Al-Shurbaji, A., Tornqvist, H., and Eriksson, J. W. (2014) Diacylglycerol acyltransferase 1 inhibition with AZD7687 alters lipid handling and hormone secretion in the gut with intolerable side effects: a randomized clinical trial. *Diabetes Obes. Metab.* **16,** 334–343 CrossRef Medline
75. DeVita, R. J., and Pinto, S. (2013) Current status of the research and development of diacylglycerol *O*-acyltransferase 1 (DGAT1) inhibitors. *J. Med. Chem.* **56,** 9820–9825 CrossRef Medline
76. Imbriglio, J. E., Shen, D. M., Liang, R., Marby, K., You, M., Youm, H. W., Feng, Z., London, C., Xiong, Y., Tata, J., Verras, A., Garcia-Calvo, M., Song, X., Addona, G. H., McLaren, D. G., *et al.* (2015) Discovery and pharmacology of a novel class of diacylglycerol acyltransferase 2 inhibitors. *J. Med. Chem.* **58,** 9345–9353 CrossRef Medline
77. Garg, A. (2004) Acquired and inherited lipodystrophies. *N. Engl. J. Med.* **350,** 1220–1234 CrossRef Medline
78. Savage, D. B. (2009) Mouse models of inherited lipodystrophy. *Dis. Model. Mech.* **2,** 554–562 CrossRef Medline
79. Huang-Doran, I., Sleigh, A., Rochford, J. J., O'Rahilly, S., and Savage, D. B. (2010) Lipodystrophy: metabolic insights from a rare disorder. *J. Endocrinol.* **207,** 245–255 CrossRef Medline
80. Hayek, T., Ito, Y., Azrolan, N., Verdery, R. B., Aalto-Setälä, K., Walsh, A., and Breslow, J. L. (1993) Dietary fat increases high density lipoprotein (HDL) levels both by increasing the transport rates and decreasing the fractional catabolic rates of HDL cholesterol ester and apolipoprotein (Apo) A-I: presentation of a new animal model and mechanistic studies in human Apo A-I transgenic and control mice. *J. Clin. Invest.* **91,** 1665–1671 CrossRef Medline
81. Escolà-Gil, J. C., Llaverias, G., Julve, J., Jauhiainen, M., Méndez-Gonzalez, J., and Blanco-Vaca, F. (2011) The cholesterol content of Western diets plays a major role in the paradoxical increase in high-density lipoprotein cholesterol and upregulates the macrophage reverse cholesterol transport pathway. *Arterioscler. Thromb. Vasc. Biol.* **31,** 2493–2499 CrossRef Medline
82. Yang, Z. H., Miyahara, H., Takeo, J., and Katayama, M. (2012) Diet high in fat and sucrose induces rapid onset of obesity-related metabolic syndrome partly through rapid response of genes involved in lipogenesis, insulin signalling and inflammation in mice. *Diabetol. Metab. Syndr.* **4,** 32 CrossRef Medline
83. Agellon, L. B., Walsh, A., Hayek, T., Moulin, P., Jiang, X. C., Shelanski, S. A., Breslow, J. L., and Tall, A. R. (1991) Reduced high density lipoprotein cholesterol in human cholesteryl ester transfer protein transgenic mice. *J. Biol. Chem.* **266,** 10796–10801 Medline
84. Williamson, R., Lee, D., Hagaman, J., and Maeda, N. (1992) Marked reduction of high density lipoprotein cholesterol in mice genetically modified to lack apolipoprotein A-I. *Proc. Natl. Acad. Sci. U.S.A.* **89,** 7134–7138 CrossRef Medline
85. Mehrabian, M., Qiao, J. H., Hyman, R., Ruddle, D., Laughton, C., and Lusis, A. J. (1993) Influence of the apoA-II gene locus on HDL levels and fatty streak development in mice. *Arterioscler. Thromb.* **13,** 1–10 CrossRef Medline
86. Imaizumi, S., Navab, M., Morgantini, C., Charles-Schoeman, C., Su, F., Gao, F., Kwon, M., Ganapathy, E., Meriwether, D., Farias-Eisner, R., Fogelman, A. M., and Reddy, S. T. (2011) Dysfunctional high-density lipoprotein and the potential of apolipoprotein A-1 mimetic peptides to normalize the composition and function of lipoproteins. *Circ. J.* **75,** 1533–1538 CrossRef Medline
87. Paigen, B., Mitchell, D., Holmes, P. A., and Albee, D. (1987) Genetic analysis of strains C57BL/6J and BALB/cJ for Ath-1, a gene determining atherosclerosis susceptibility in mice. *Biochem. Genet.* **25,** 881–892 CrossRef Medline
88. Ishida, B. Y., Blanche, P. J., Nichols, A. V., Yashar, M., and Paigen, B. (1991) Effects of atherogenic diet consumption on lipoproteins in mouse strains C57BL/6 and C3H. *J. Lipid Res.* **32,** 559–568 Medline
89. Ferrell, J. M., Boehme, S., Li, F., and Chiang, J. Y. (2016) Cholesterol 7α-hydroxylase-deficient mice are protected from high-fat/high-cholesterol diet-induced metabolic disorders. *J. Lipid Res.* **57,** 1144–1154 CrossRef Medline
90. Gonzalez, F. J., Jiang, C., Xie, C., and Patterson, A. D. (2017) Intestinal farnesoid X receptor signaling modulates metabolic disease. *Dig. Dis.* **35,** 178–184 CrossRef Medline
91. Woo, Y. C., Xu, A., Wang, Y., and Lam, K. S. (2013) Fibroblast growth factor 21 as an emerging metabolic regulator: clinical perspectives. *Clin. Endocrinol.* **78,** 489–496 CrossRef Medline
92. Ni, D., Xu, P., and Gallagher, S. (2017) Immunoblotting and immunodetection. *Curr. Protoc. Protein Sci.* **88,** 10.10.1–10.10.37 Medline
93. Bradford, M. M. (1976) A rapid and sensitive method for the quantitation of microgram quantities of protein utilizing the principle of protein-dye binding. *Anal. Biochem.* **72,** 248–254 CrossRef Medline
94. Eder, K., Reichlmayr-Lais, A. M., and Kirchgessner, M. (1993) Studies on the extraction of phospholipids from erythrocyte membranes in the rat. *Clin. Chim. Acta* **219,** 93–104 CrossRef Medline
95. Theise, N. D. (2007) Liver biopsy assessment in chronic viral hepatitis: a personal, practical approach. *Mod. Pathol.* **20,** S3–S14 CrossRef Medline
96. Bligh, E. G., and Dyer, W. J. (1959) A rapid method of total lipid extraction and purification. *Can. J. Biochem. Physiol.* **37,** 911–917 CrossRef Medline
97. McDonough, V. M., and Roth, T. M. (2004) Growth temperature affects accumulation of exogenous fatty acids and fatty acid composition in *Schizosaccharomyces pombe*. *Antonie Van Leeuwenhoek* **86,** 349–354 CrossRef Medline